Cell Stem Cell

Article

Leukemogenic Chromatin Alterations Promote AML Leukemia Stem Cells via a KDM4C-ALKBH5-AXL Signaling Axis

Graphical Abstract

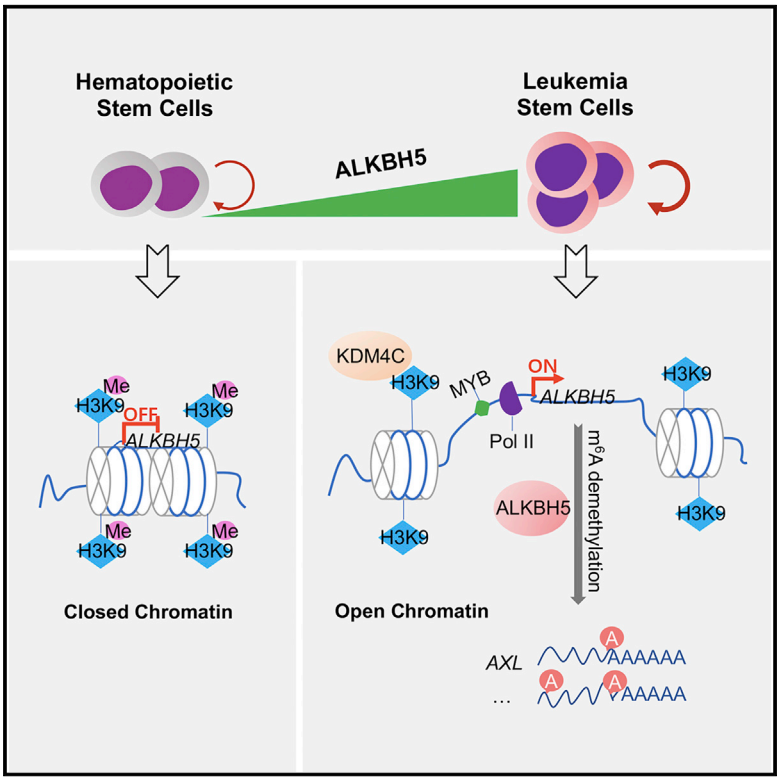

Highlights

- ALKBH5 is highly expressed in AML and associated with poor prognosis
- ALKBH5 is selectively required for LSCs but dispensable for normal HSCs
- KDM4C regulates ALKBH5 expression by increasing chromatin accessibility to MYC and Pol II
- ALKBH5 affects mRNA stability of AXL in an m^{6}A-dependent manner

Authors

Jiazhen Wang, Yicun Li, Peipei Wang, ..., Yi Luo, Shaoguang Li, Haojian Zhang

Correspondence

haojian_zhang@whu.edu.cn

In Brief

Wang et al. find that ALKBH5 is specifically required for maintaining the function of acute myeloid leukemia (AML) stem cells but not normal hematopoietic stem cells and reveal KDM4C-ALKBH5-AXL signaling axis in AML development and maintenance. These findings lay the foundation for targeting ALKBH5 for AML therapy.

Wang et al., 2020, Cell Stem Cell *27*, 81–97
July 2, 2020
https://doi.org/10.1016/j.stem.2020.04.001

CellPress

Cell Stem Cell

CellPress

Article

Leukemogenic Chromatin Alterations Promote AML Leukemia Stem Cells via a KDM4C-ALKBH5-AXL Signaling Axis

Jiazhen Wang,[1,2,10] Yicun Li,[1,10] Peipei Wang,[1,2,10] Guoqiang Han,[1,2,10] Tiantian Zhang,[1,2] Jiwei Chang,[1,2] Rong Yin,[1,2] Yi Shan,[3] Jin Wen,[4] Xueqin Xie,[1,2] Mengdie Feng,[1,2] Qifan Wang,[1,2] Jin Hu,[1,2] Ying Cheng,[1,2] Tong Zhang,[1,2] Yashu Li,[1,2] Zhuying Gao,[1,2] Chengli Guo,[1] Jing Wang,[1] Jianfei Liang,[1] Manman Cui,[1,2] Kexin Gao,[1,2] Jihua Chai,[1] Weidong Liu,[1] Hui Cheng,[5,6] Lei Li,[7] Fuling Zhou,[8] Lingbo Liu,[4] Yi Luo,[9] Shaoguang Li,[3] and Haojian Zhang[1,2,11,*]

[1]The State Key Laboratory Breeding Base of Basic Science of Stomatology & Key Laboratory of Oral Biomedicine Ministry of Education, School & Hospital of Stomatology, Wuhan University, Wuhan, China

[2]Frontier Science Center for Immunology and Metabolism, Medical Research Institute, School of Medicine, Wuhan University, Wuhan, China

[3]Division of Hematology/Oncology, Department of Medicine, University of Massachusetts Medical School, Worcester, MA, USA

[4]Institute of Hematology, Union Hospital, Tongji Medical College, Huazhong University of Science and Technology, Wuhan, China

[5]State Key Laboratory of Experimental Hematology, Tianjin, China

[6]Institute of Hematology and Blood Disease Hospital, Chinese Academy of Medical Sciences, Peking Union Medical College, Tianjin, China

[7]Department of Pediatrics, Union Hospital, Huazhong University of Science and Technology, Wuhan, China

[8]Department of Hematology, Zhongnan Hospital, Wuhan University, Wuhan, China

[9]Department of Hematology, Tongji Hospital, Tongji Medical College, Huazhong University of Science and Technology, Wuhan, China

[10]These authors contributed equally

[11]Lead Contact

*Correspondence: haojian_zhang@whu.edu.cn

https://doi.org/10.1016/j.stem.2020.04.001

SUMMARY

N^6-methyladenosine (m^{6}A) is a commonly present modification of mammalian mRNAs and plays key roles in various cellular processes. m^{6}A modifiers catalyze this reversible modification. However, the underlying mechanisms by which these m^{6}A modifiers are regulated remain elusive. Here we show that expression of m^{6}A demethylase ALKBH5 is regulated by chromatin state alteration during leukemogenesis of human acute myeloid leukemia (AML), and ALKBH5 is required for maintaining leukemia stem cell (LSC) function but is dispensable for normal hematopoiesis. Mechanistically, KDM4C regulates ALKBH5 expression via increasing chromatin accessibility of *ALKBH5* locus, by reducing H3K9me3 levels and promoting recruitment of MYB and Pol II. Moreover, ALKBH5 affects mRNA stability of receptor tyrosine kinase *AXL* in an m^{6}A-dependent way. Thus, our findings link chromatin state dynamics with expression regulation of m^{6}A modifiers and uncover a selective and critical role of ALKBH5 in AML that might act as a therapeutic target of specific targeting LSCs.

INTRODUCTION

Acute myeloid leukemia (AML) is an aggressive and fatal hematologic malignancy characterized by uncontrolled expansion of poorly differentiated myeloid cells (Döhner et al., 2015). The development of AML is associated with accumulation of acquired genetic and epigenetic changes in hematopoietic stem/progenitor cells (HSPCs) (Ley et al., 2013; Shlush et al., 2014). Increasing evidence demonstrates that acquisition of some founder mutations in HSPCs may create a unique cellular state, known as pre-leukemic hematopoietic stem cells (HSCs), which display multilineage repopulation advantage and expand to form pre-leukemic clones (Shlush et al., 2014). Subsequent acquisitions of additional genetic or epigenetic changes in pre-leukemic HSCs (pHSCs) establish their cellular identity as leukemia stem cells (LSCs), which are responsible for leukemia initiation, progression, and relapse (Eppert et al., 2011; Shlush et al., 2014, 2017). Despite the progress made in understanding the molecular basis of AML development, overall survival of adult patients has not significantly improved in the past three decades. Thus, it is critical to explore distinct mechanisms during leukemogenesis at a molecular level for a better understanding of AML pathogenesis that will lead to the development of potentially effective therapeutic strategies.

Chromatin states are crucial for defining cellular identity (Cusanovich et al., 2018; Lara-Astiaso et al., 2014; Yoshida et al., 2019). Cancer cells have aberrant epigenetic landscapes and often exploit chromatin machinery to dysregulate gene expression (Chi et al., 2010; Garraway and Lander, 2013). Similarly, leukemia cells display unique chromatin accessibility that can guide

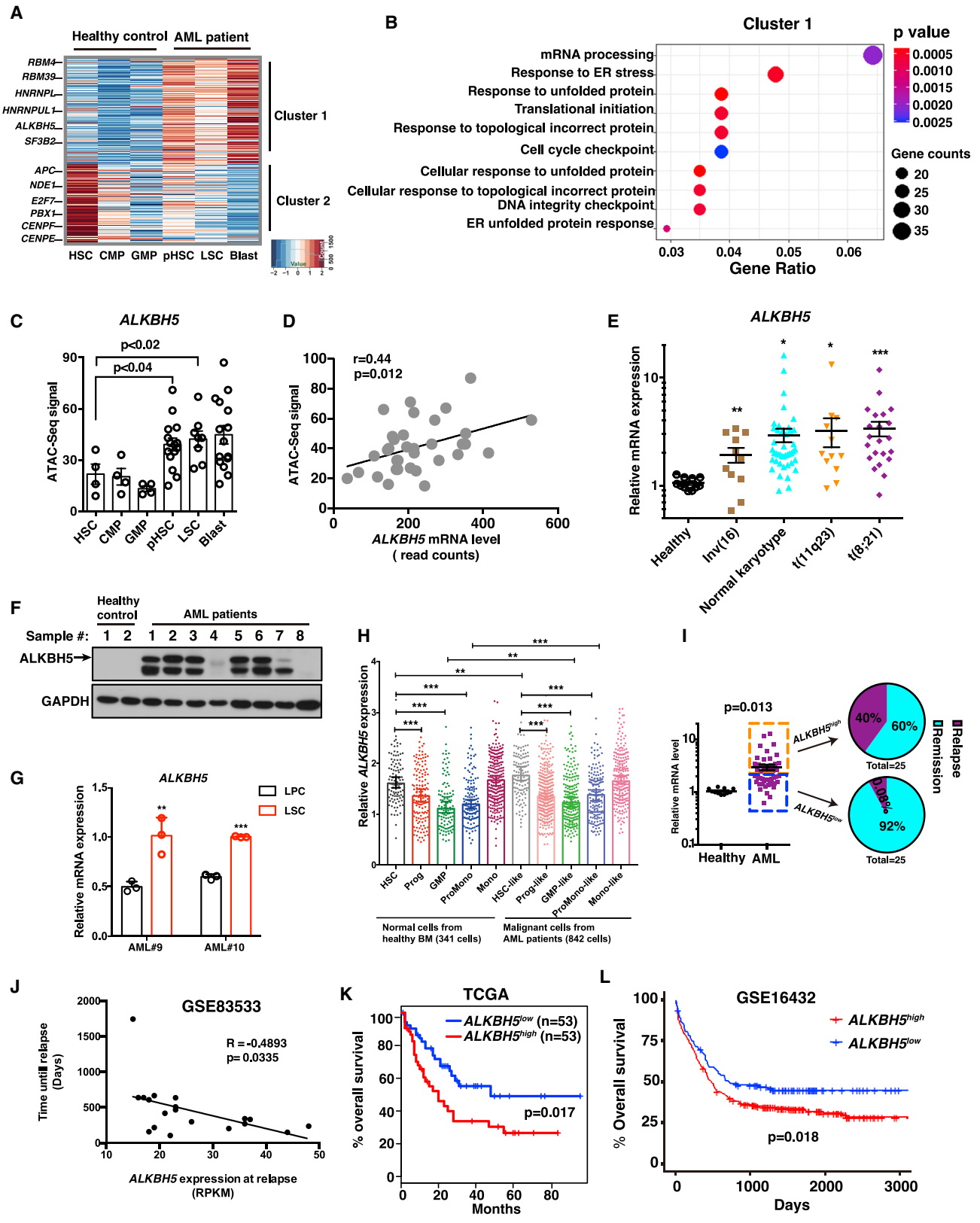

(legend on next page)

cell-fate programs by altering the regulatory networks (Chen et al., 2015; Cheung et al., 2016; Jing et al., 2018). Therefore, it is speculated that genes susceptible to chromatin state changes may play key roles in leukemogenesis.

N^6-methyladenosine (m^6A) is a commonly present modification of mammalian mRNAs (Desrosiers et al., 1974), and recent evidence indicates that m^6A plays crucial roles in various cellular processes (Cui et al., 2017; Dominissini et al., 2012; Han et al., 2019; Li et al., 2017a; Mauer et al., 2017; Meyer and Jaffrey, 2014; Meyer et al., 2012; Shi et al., 2018; Winkler et al., 2019; Xiang et al., 2017; Zhou et al., 2015). This reversible modification is catalyzed by m^6A modifiers including methyltransferase complex (METTL3-METTL14-WTAP) (Liu et al., 2014) and two demethylases, ALKBH5 (Zheng et al., 2013) and FTO (Jia et al., 2011). Although the expression of some of these m^6A modifiers is dysregulated in tumor pathogenesis (Barbieri et al., 2017; Li et al., 2017b; Vu et al., 2017a; Weng et al., 2018; Zhang et al., 2017), the underlying mechanisms by which these m^6A modifiers are regulated remain poorly understood. ALKBH5 belongs to the AlkB family of α-ketoglutarate-dependent dioxygenases and is a major m^6A demethylase (Zheng et al., 2013). However, the role of ALKBH5 in leukemogenesis remains elusive. Here, we show that chromatin state substantially affects ALKBH5 expression during leukemogenesis, and ALKBH5 is selectively required for maintaining the function of AML LSCs.

RESULTS

The *ALKBH5* Locus Displays Increased Chromatin Accessibility during Leukemogenesis and Is Highly Active in AML LSCs

To investigate the genetic changes due to chromatin state alterations, we first interrogated chromatin accessibility dynamics in AML patient-derived pHSCs, LSCs, leukemic blast cells (blasts), as well as, in healthy donor-derived HSCs, common myeloid progenitors (CMPs) and granulocyte/macrophage progenitors (GMPs) from publicly available datasets of assay for transposase-accessible chromatin using sequencing (ATAC-seq) (Corces et al., 2016). We observed that substantial chromatin remodeling occurred when cells transformed from normal HSCs to pHSCs, LSCs, and blasts (Figure 1A). *k*-means clustering analysis revealed two trends of chromatin accessibility alterations during leukemogenesis: gained accessibility (cluster 1) and gradually lost accessibility (cluster 2). Notably, genes in cluster 1 involved in several biological processes, such as mRNA processing, response to ER stress, response to unfolded protein, and translational initiation (Figure 1B), whereas genes in cluster 2 were enriched in regulation of cell cycle phase transitions (Figure S1A). These results indicate that chromatin state alteration affects multiple genetic programs in human AML development.

Recent studies have uncovered critical roles of mRNA processing, such as m^6A modification, in AML development (Dolnik et al., 2012; Vu et al., 2017b; Wang et al., 2019; Weng et al., 2018). Interestingly, we found that m^6A demethylase, *ALKBH5*, but not other m^6A modifiers (*METTL3*, *METTL14*, *WTAP*, and *FTO*), belonged to cluster 1, displaying significantly higher chromatin accessibility in the populations of AML patient-derived pHSCs, LSCs, and blasts than in normal HSCs, CMPs, and GMPs (Figures 1C and S1B–S1G). In these cells, the degree of chromatin openness of *ALKBH5* locus positively correlated with its transcript level (Figures 1D and S1H), suggesting that *ALKBH5* expression was actively regulated by chromatin accessibility during leukemogenesis. In addition, we observed that *ALKBH5* was expressed at a significantly higher level in leukemia cells from AML patients, including patients with normal karyotype, inv(16), *MLL*-rearranged t(11q23), and t(8,21), compared with healthy donor controls (Figure 1E). A similar result was observed by analyzing published datasets (Figure S1I). We also found that ALKBH5 was aberrantly overexpressed in most AML patient samples (Figures 1F and S1J). Importantly, the highest expression of *ALKBH5* was detected mainly in LSCs (Figures 1G and S1K). We further used single-cell RNA sequencing (RNA-seq) and genotyping at the single-cell level to compare *ALKBH5* expression between primitive AML cells and normal controls (van Galen et al., 2019). We found that primitive AML cells from patients (including HSC-like, Prog-like, and GMP-like malignant cells) exhibited higher expression of *ALKBH5* than their counterparts (HSCs, Progs, and GMPs) from healthy bone marrow (Figure 1H). Thus, these results suggest that ALKBH5 expression is determined by alterations in chromatin accessibility during leukemogenesis. Higher

Figure 1. The *ALKBH5* Locus Displays Increased Chromatin Accessibility during Leukemogenesis and Is Highly Active in LSCs, Associated with Poor Prognosis

(A) *k*-Means clustering of ATAC-seq data (GSE74912) showing alterations of chromatin accessibility in normal human HSPCs and AML patient-derived pHSCs, LSCs, and blasts.

(B) Gene Ontology analysis of genes in cluster 1.

(C) Normalized ATAC-seq signal at the *ALKBH5* locus in HSCs, CMPs, GMPs, pHSCs, LSCs, and blasts. Each dot represents one individual AML patient sample.

(D) Pearson's correlation of *ALKBH5* expression levels with the degree of its chromatin accessibility in AML patient-derived pHSCs, LSCs, and blasts.

(E) qRT-PCR analysis showing *ALKBH5* expression in normal bone marrow cells from healthy donors (n = 11) and in AML patient-derived primary leukemia cells (n = 88).

(F) Immunoblot showing ALKBH5 expression in bulk bone marrow mononuclear cells from healthy donors (n = 2) and AML patients (n = 8) using GAPDH as an internal loading control.

(G) qRT-PCR analysis of *ALKBH5* expression in leukemia progenitor cells (LPCs) and LSCs sorted from two independent AML patients.

(H) Single-cell RNA-seq data showing *ALKBH5* expression in healthy donor- and AML patient-derived bone marrow cells. Each dot represents one cell.

(I) Proportion of remission and relapse of two AML patient groups ($ALKBH5^{high}$ [n = 25] and $ALKBH5^{low}$ [n = 25]) divided by *ALKBH5* expression.

(J) Pearson's correlation between *ALKBH5* expression and days to relapse of AML patients (GSE83553; n = 19).

(K and L) Kaplan-Meier plots of overall survival in TCGA (K) and GSE16432 (L) cohorts for AML patients, stratified on the basis of *ALKBH5* expression above ($ALKBH5^{high}$) or below ($ALKBH5^{low}$) the median.

*p < 0.05, **p < 0.01, and ***p < 0.001 (t test). Error bars denote mean ± SEM.

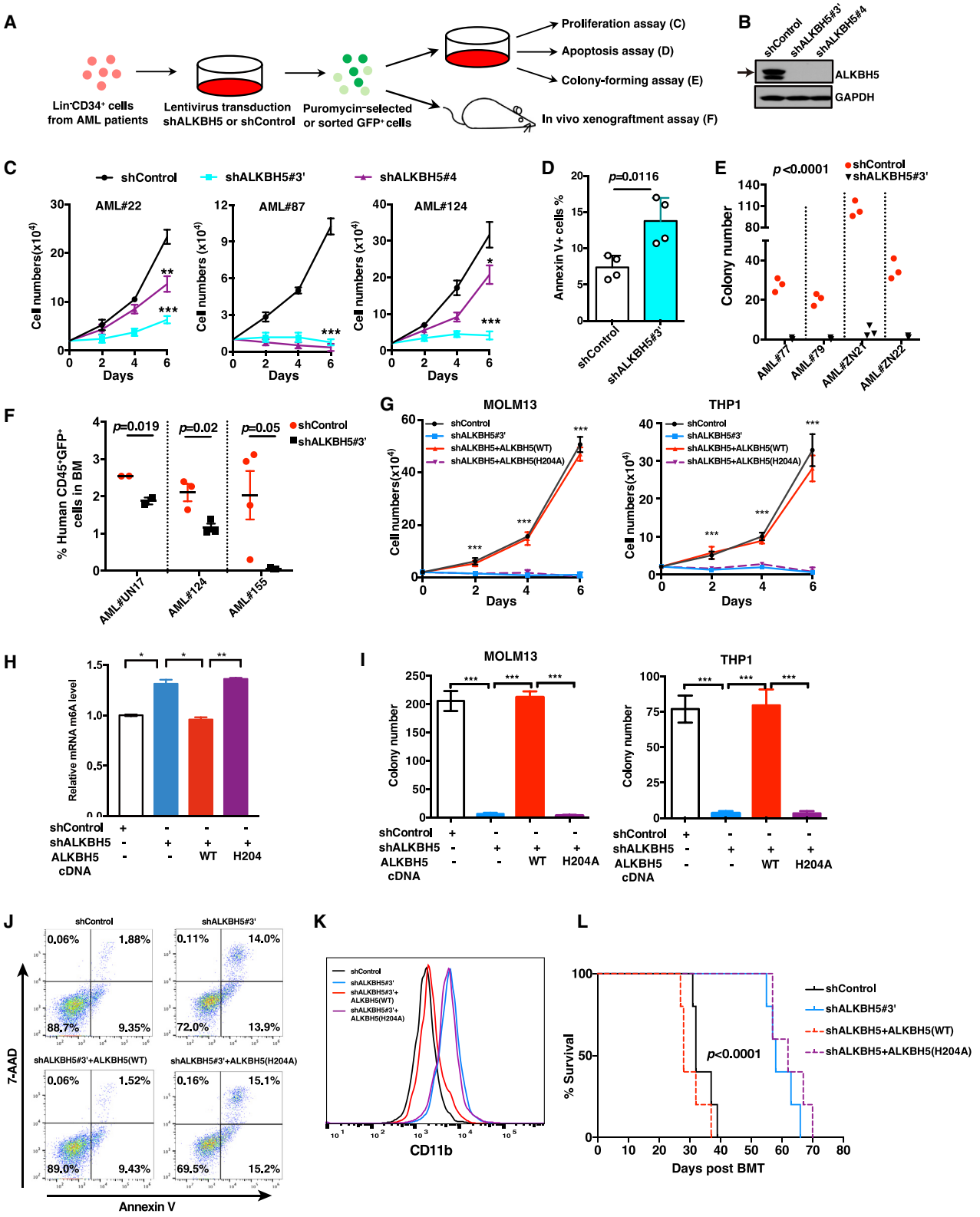

Figure 2. ALKBH5 Is Required for Maintaining Primary Human AML LSC Capability

(A) Experimental scheme for (B)–(F).

(B) Immunoblot showing knockdown efficiency of ALKBH5 in leukemia cells.

(legend continued on next page)

expression of ALKBH5 in LSCs implies that it plays a key role in regulating the function of AML LSCs.

Higher ALKBH5 Expression Is Associated with Poor Prognosis of AML

Next, we investigated the prognostic value of ALKBH5 in AML. We observed that *ALKBH5* expression was consistently higher in the relapse samples versus their paired diagnostic samples (Figure S1L). On the basis of the levels of *ALKBH5* expression, we further stratified patients (with sufficient response data available) as remission or relapse and found that increased *ALKBH5* expression was associated with significantly higher relapse percentage (40% in the *ALKBH5*^{high} cohort versus 0.08% in the *ALKBH5*^{low} cohort) (Figure 1I). Similarly, *ALKBH5* expression levels negatively correlated with duration until relapse (Figure 1J). These data suggest that AML patients with high *ALKBH5* expression may survive chemotherapy but suffer relapse. To support this idea, we further studied two AML patient cohorts and found that elevated expression of *ALKBH5* correlated with overall shorter survival of AML patients (Figures 1K and 1L). Collectively, these data demonstrated that higher ALKBH5 expression correlates with poor prognosis of AML.

ALKBH5 Is Essential for Maintaining the Function of Human AML LSCs

Upregulation of ALKBH5 expression in AML LSCs promoted us to investigate its function in leukemogenesis (Figure 2A). We performed short hairpin RNA (shRNA)-mediated knockdown (KD) experiments to abrogate ALKBH5 expression. Compared with the scramble control, both shRNAs markedly knocked down ALKBH5 expression, accompanied by an increase in global m^{6}A levels (Figures 2B and S2A). To determine ALKBH5 function, we first used human myeloid leukemia cell lines and found that ALKBH5 KD significantly blocked cellular growth and inhibited the clonogenicity (Figures S2B and S2C). Additionally, CRISPR/Cas9-mediated knockout of ALKBH5 also showed marked inhibition of cellular growth (Figure S2D). Next, we used AML patient-derived primary Lin$^-$CD34$^+$ cells, which are commonly considered an LSC-enriched population. Compared with the control group, ALKBH5 KD significantly inhibited proliferation, induced cell apoptosis, and reduced colony formation (Figures 2C–2E). We also examined the *in vivo* leukemia reconstitution ability of AML LSCs by using xenograft assay. As expected, ALKBH5 KD significantly reduced the leukemogenic potential of the cells in immune-deficient mice (Figure 2F). Together, these results indicate that ALKBH5 is required to maintain the function of human AML LSCs.

Demethylation Activity of ALKBH5 Is Required for Survival of Human Leukemia Cells

To rule out off-target possibility and determine whether enzymatic activity was required for ALKBH5 function, we restored *ALKBH5* expression by inserting its cDNA resistant to shALKBH5#3′ targeting the 3′ UTR (Figure S2E). We observed that restoration of wild-type (WT) *ALKBH5* substantially rescued the cellular growth and clonogenicity of human AML cell lines MOLM-13 and THP1 (Figures S2F–S2I), suggesting that the inhibitory effects of ALKBH5 deficiency were not caused by the off-target effects of shRNAs. The *ALKBH5* mutant, which carried the H204A mutation to disrupt its enzymatic activity (Zheng et al., 2013), was also used in the rescue experiment. Our results showed that the *ALKBH5* mutant failed to rescue the defects in cellular growth and clonogenic ability of human leukemia cells caused by ALKBH5 deficiency (Figures 2G–2I), indicating that ALKBH5 enzymatic activity is required for its function in promoting AML cell survival. Furthermore, *ALKBH5* KD caused cell-cycle arrest, promoted differentiation, and induced apoptosis of the leukemia cells. These biological changes were also rescued by WT *ALKBH5*, but not the mutant that lacked enzymatic activity (Figures 2J, 2K, S2K, and S2L). Furthermore, ALKBH5-KD cells exhibited delayed leukemia development *in vivo*, which was reversed by restoration of expression of WT ALKBH5, but not its mutant lacking the enzymatic activity (Figures 2L and S2J). Together, these results indicate that ALKBH5, along with an intact demethylase activity, is required for survival and stem cell maintenance of human AML cells.

Alkbh5 Is Required for Murine AML Development and Maintenance of LSCs

To test whether Alkbh5 is required for murine leukemogenesis, we generated *Alkbh5*$^{fl/fl}$ mice and crossed with an Mx1-Cre strain to produce *Mx1-cre;Alkbh5*$^{fl/fl}$ mice (Figure S3A). Efficient deletion of *Alkbh5* was observed 2 weeks after the last polyinosinic-polycytidylic acid (pIpC) injection (Figure S3B). For simplicity, pIpC-treated *Mx1-cre;Alkbh5*$^{fl/fl}$ mice will be referred to as *Alkbh5*$^{-/-}$ mice and pIpC-treated *Alkbh5*$^{fl/fl}$ control mice as WT mice.

We first studied the role of *Alkbh5* in AML development. Lin$^-$ bone marrow cells from WT and *Alkbh5*$^{-/-}$ mice were transduced with MLL-AF9-YFP retrovirus and then transplanted into

(C) Growth curves of AML patient-derived Lin$^-$CD34$^+$ cells after ALKBH5 knockdown.
(D) Percentage of apoptotic cells (annexin V$^+$) cells (n = 2 biologically independent samples, with two independent cultures each [n = 4]).
(E) Colony-forming unit assay using primary Lin$^-$CD34$^+$ cells from four individual AML patients after knockdown of ALKBH5. Each dot represents one culture (n = 24).
(F) *In vivo* leukemic engraftment analysis at 10–12 weeks after xenotransplantation. Data are combined from three independent experiments for three AML patients (two to four recipients per patient per group).
(G) Growth curves of leukemia cells after transduction with indicated lentiviruses.
(H) Quantification of mRNA m^{6}A levels in MOLM-13 cells after transduction with indicated lentiviruses.
(I) Colony-forming unit assay of MOLM-13 and THP1 cells after transduction with indicated lentiviruses.
(J) Apoptotic analysis of MOLM-13 cells transduced with indicated lentiviruses.
(K) Flow cytometry analysis of differentiation of MOLM-13 cells (CD11b$^+$).
(L) Kaplan-Meier survival plot of recipients transplanted with MOLM-13 cells transduced with indicated lentiviruses (n = 4 or 5 recipients per group).
*p < 0.05, **p < 0.01, and ***p < 0.001 (t test). Error bars denote mean ± SEM.

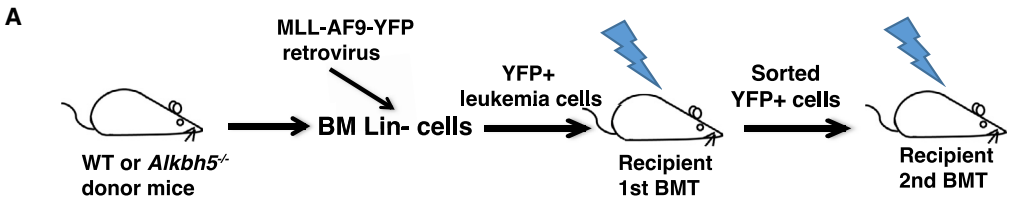

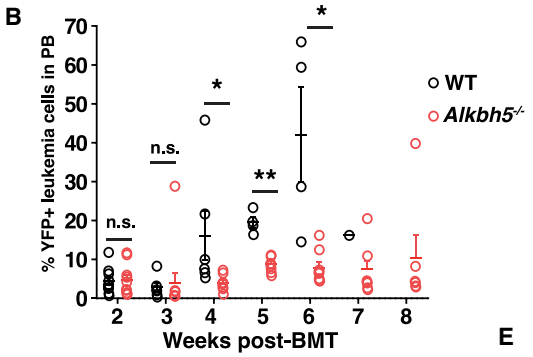

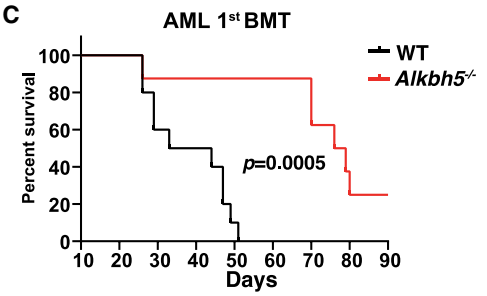

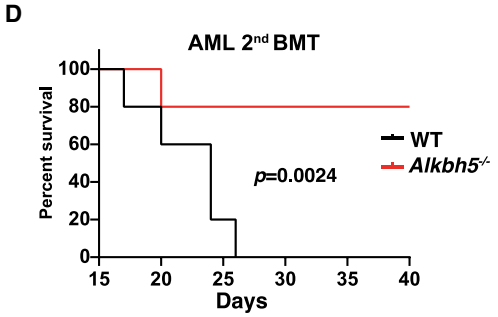

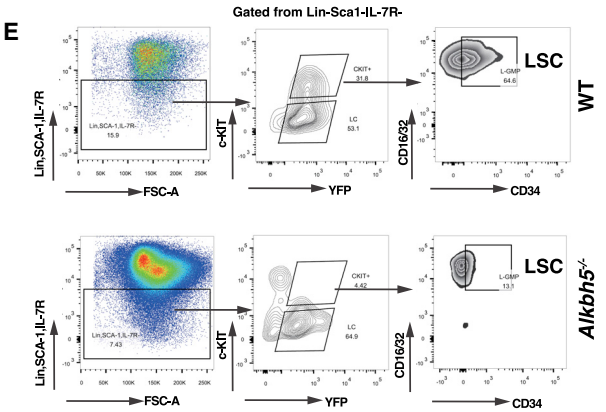

F

Limiting Dilution Assay

Cell No.	WT	*Alkbh5*$^{-/-}$
50K	5/5	5/5
10K	5/5	4/5
2 K	5/5	1/5
0.4K	3/5	0/5

LSC Frequency

Group	Lower	Estimate	Upper
WT	1/1121	1/410	1/150
Alkbh5$^{-/-}$	1/17559	1/7249	1/2993

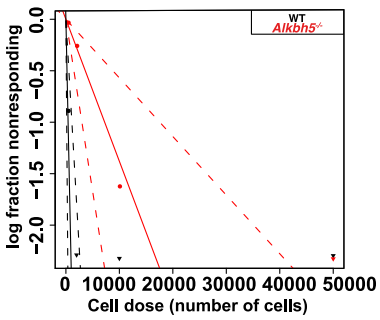

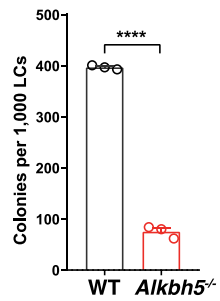

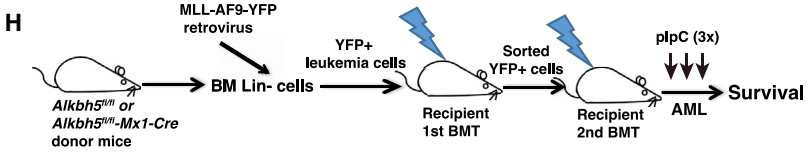

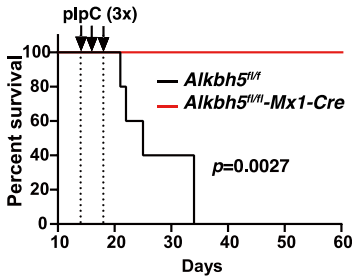

(legend on next page)

lethally irradiated recipient mice (Figure 3A). Recipients of MLL-AF9-transduced *Alkbh5*$^{-/-}$ Lin$^-$ cells developed and died of AML significantly slower than did recipients of MLL-AF9-transduced WT Lin$^-$ cells (Figure 3C). The delayed AML development in the absence of Alkbh5 correlated with a lower percentage of leukemia cells in the peripheral blood (PB) and less severe splenomegaly (Figures 3B, S3C, and S3D). Thus, these data indicate that Alkbh5 is required for AML development.

Next, we explored the role of Alkbh5 in maintaining LSC function. Alkbh5 deletion significantly impaired the ability of LSCs to cause disease in secondary recipient mice (Figures 3D and S3D). Additionally, we observed a dramatically lower percentage of LSCs in the absence of *Alkbh5* (Figure 3E). To directly enumerate the frequency of LSCs, we performed a limiting dilution assay. The frequency of LSCs in *Alkbh5*$^{-/-}$ AML mice was lower compared with the WT group (1:7,249 versus 1:410 cells) (Figures 3F and S3E). This was also confirmed by a colony-forming unit (CFU) assay showing a lesser number of colonies in the absence of Alkbh5 (Figure 3G). We further asked whether acute deletion of *Alkbh5* from established LSCs affects leukemia maintenance. We first induced leukemia initiation using MLL-AF9-transduced Lin$^-$ cells from *Alkbh5*$^{fl/fl}$ *and Mx1-cre;Alkbh5*$^{fl/fl}$ mice. To rule out the issue of Mx1-Cre leakiness, we sorted YFP$^+$ leukemia cells from primary recipients and transplanted them into secondary recipients. Fourteen days following leukemia engraftment, deletion of Alkbh5 was induced by injecting recipients with pIpC (Figure 3H). As expected, acute deletion of Alkbh5 inhibited leukemia propagation (Figure 3I), suggesting that Alkbh5 is critical for LSC maintenance. Together, our data indicate that Alkbh5 is required for the development of murine AML and maintenance of LSC function.

ALKBH5 Is Dispensable for Normal Human CD34$^+$ HSPCs and Murine Hematopoiesis

Next, we explored whether ALKBH5 is required for normal hematopoietic function. First, we knocked down ALKBH5 by shRNAs in human cord blood-derived CD34$^+$ cells and observed comparable colony-forming ability and myeloid differentiation (Figure 4A), indicating that ALKBH5 is not required for the function of normal human CD34$^+$ HSPCs. We further examined the effects of Alkbh5 on HSC function and normal hematopoiesis using *Alkbh5*$^{-/-}$ mice. Compared with WT mice, *Alkbh5*$^{-/-}$ mice showed similar blood counts and percentages of different types of blood cells in the PB, including white blood cells (WBCs), lymphocytes (LYMs), granulocytes (GRAs), monocytes (MONs), platelets, and red blood cells (RBCs), at 2 and 4 weeks after the last pIpC injection (Figures 4B, 4C, S4A, and S4B). Furthermore, deletion of Alkbh5 did not cause a significant change in bone marrow cellularity (Figures 4D and S4C) and showed similar spleen weight as WT mice (Figure S4D). Next, we observed that the percentages and total numbers of LT-HSC, ST-HSC, MPP2, MPP3, MPP4, LSK, LMPP, progenitor, CMP, GMP, MEP, and CLP in the bone marrow of *Alkbh5*$^{-/-}$ mice were similar to those in WT mice (Figures 4E–4H and S4E–S4H). Thus, these data indicate that ALKBH5 is not required for normal hematopoiesis.

We next investigated the effects of Alkbh5 on HSC function. A CFU assay showed normal clonogenicity and differentiation potential of *Alkbh5*$^{-/-}$ stem/progenitor cells (Figure 4I). Furthermore, we performed a competitive repopulation assay to determine whether Alkbh5 affects the self-renewal capacity of HSCs. These chimeric mice were analyzed using flow cytometry over 4–16 weeks after bone marrow transplantation (BMT). The percentages of donor-derived total cells (CD45.2$^+$), myeloid cells (Mac1$^+$, Gr-1$^+$), T cells (CD3e+), and B cells (B220+) in PB were similar (Figure 4J), suggesting that *Alkbh5*$^{-/-}$ HSCs have a reconstitution ability that is comparable with WT controls. At 16 weeks, we also did not observe any significant differences in the percentages of donor-derived stem and progenitor populations in the recipients (Figures 4K and 4L). To test the long-term function of HSCs, we sorted donor-derived LSK cells from the above recipients at 16 weeks and performed secondary transplantation. We observed similar percentages of donor-derived different lineage cells in the PB of recipients over 4–12 weeks after BMT (Figure 4M). Together, these results indicate that Alkbh5 does not affect the function of normal HSCs.

ALKBH5 Expression Is Regulated by Epigenetic Alterations in Human AML Cells

Because histone modifications modulate the local structure of chromatin and influence gene expression, by regulating the accessibility of gene loci to transcriptional machinery (Tessarz and Kouzarides, 2014), we reasoned that ALKBH5 expression could be affected by chromatin accessibility during AML development. We first interrogated epigenetic dynamics of leukemia cells by analyzing publicly available datasets (Chen et al., 2015; Wong et al., 2015). We found that the promoter regions of all m^{6}A modifiers had significantly high levels of the active histone marks H3K9ac, H3K4me3, H3K4me2, and H3K79me2 and a lower level of the repressive histone mark H3K27me3 in murine c-kit$^+$ leukemia-initiating cells (LICs) (Figures S5A–S5G). Of all these epigenetic changes, the *Alkbh5* locus showed the highest

Figure 3. Alkbh5 Is Required for Murine AML Development and Maintenance of LSC Function

(A) Experimental scheme for MLL-AF9 induced murine AML model. BMT, bone marrow transplantation.

(B) Percentages of YFP$^+$ leukemia cells in PB at the indicated time after transplantation (n = 5 per group).

(C) Kaplan-Meier survival curves for recipients of MLL-AF9-transduced Lin$^-$ bone marrow cells from WT (n = 8) or *Alkbh5*$^{-/-}$ (n = 9) donor mice.

(D) Kaplan-Meier survival curves for secondary BMT recipient mice receiving equal number of YFP$^+$ leukemia cells from primary AML mice (n = 5 for WT and *Alkbh5*$^{-/-}$).

(E) Representative flow plot showing the percentage of LSCs in recipient mice from secondary BMT for WT and *Alkbh5*$^{-/-}$ groups.

(F) Limiting dilution assays. Table (left) shows different numbers of cells and recipient mice used for the transplant. Graph (right) shows the frequency of LSCs in WT and *Alkbh5*$^{-/-}$ AML mice.

(G) Colony-forming unit assay for leukemic cells from primary WT and *Alkbh5*$^{-/-}$ AML mice.

(H) Experimental scheme for analyzing the function of Alkbh5 in leukemia maintenance.

(I) Kaplan-Meier survival curves for leukemia maintenance assay (n = 5 for *Alkbh5*$^{fl/fl}$ and *Alkbh5*$^{fl/fl}$*;Mx1-Cre*).

*p < 0.05, **p < 0.01, and ***p < 0.001 (t test). Error bars denote mean ± SEM.

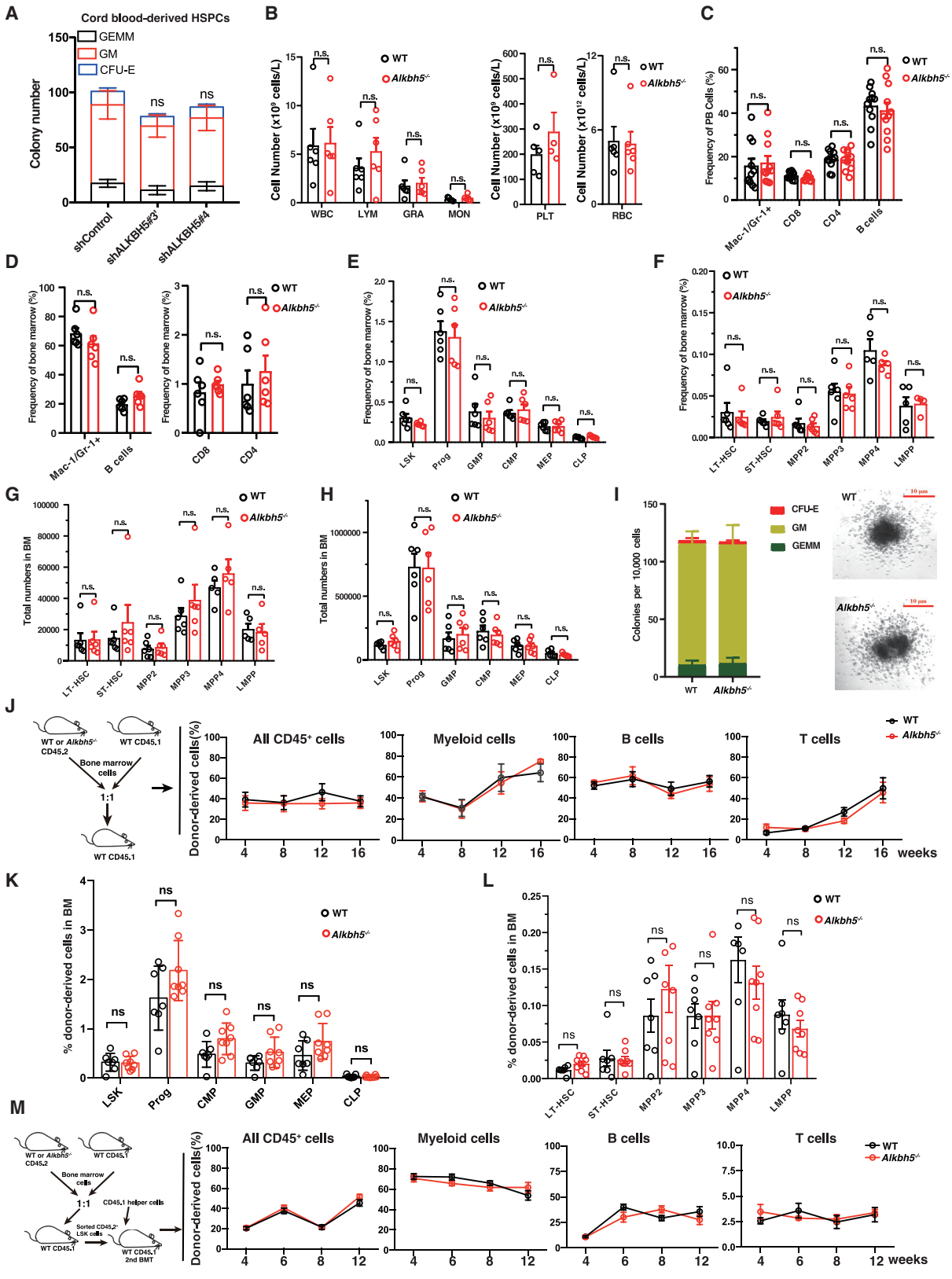

(legend on next page)

enrichment of these active histone marks and the highest degree of chromatin openness (Figure 5A). Consistently, this locus also displayed highly accessible and active in human myeloid leukemia cell K562, marked by hypersensitivity to DNase I and higher enrichment of H3K27ac, H3K4me3, and H3K4me2, which are proximal to the boundary of topological domain (Figure 5B). We further examined the chromatin state of *ALKBH5* promoter region in AML patient-derived leukemia cells using chromatin immunoprecipitation quantitative polymerase chain reaction (ChIP-qPCR). The enrichment of H3K4me3 in the *ALKBH5* promoter region was significantly increased, while the enrichment of H3K9me3 was decreased (Figure 5C). On the basis of these results, we propose that altering the chromatin state of *ALKBH5* locus could interfere with its expression.

To profile *ALKBH5* promoter-binding proteins, we performed a DNA pull-down assay in combination with mass spectrometry. As expected, we found that H3K4 histone methyltransferases, including KMT2A and KMT2B (also called MLL1 and MLL2, respectively), were enriched in this region (Figure 5D). We attempted to identify the MLLs required for regulating *ALKBH5* by KD of the four H3K4 methyltransferases, MLL1–4, individually. We found that KD of *MLL1* and *MLL3*, but not *MLL2* and *MLL4*, significantly downregulated *ALKBH5* expression (Figures S5H and S5I). In addition, H3K9 histone demethylases, including JMJD2B and JMJD1C, were accumulated in the *ALKBH5* promoter region (Figures 5D and 5E), suggesting that they are responsible for the reduction of H3K9me3 in this region in AML cells (Figure 5C). Moreover, we found enrichment of transcriptional factors RUNX2, MYB, and PBX3 in the *ALKBH5* promoter (Figures 5D and 5E). KD of *MYB* by two different shRNAs significantly decreased ALKBH5 expression in leukemia, at both the mRNA and protein levels (Figures 5F and 5G), suggesting that MYB plays a critical role in regulating ALKBH5 expression in leukemia cells. Together, these results indicate that the chromatin state determines ALKBH5 expression in human AML cells.

KDM4C Regulates ALKBH5 Expression by Modulating Chromatin Accessibility

KDM4C is a histone demethylase that removes H3K9me3 (Cheung et al., 2016). We found that KDM4C was also enriched in the *ALKBH5* promoter region (Figure 5E), implying that it is involved in regulating ALKBH5 expression. We observed that *KDM4C* expression was significantly higher in AML patient-derived leukemia cells and LSCs, which supported our speculation (Figures 5H and 5I). The level of *KDM4C* expression positively correlated with that of *ALKBH5* in leukemia cells from AML patients (Figure S5J). Moreover, KDM4C KD significantly downregulated ALKBH5 expression at both the mRNA and protein levels in leukemia cells, accompanied by an increase in the level of H3K9me3 (Figures 5J, 5K, S5K, and S5L). Similar to ALKBH5 deficiency, KDM4C KD inhibited the cellular growth and reduced the clonogenic ability of leukemia cells (Figures S5M and S5N), which supported the findings of a previous study showing that KDM4C is essential for initiation and maintenance of leukemia (Cheung et al., 2016). Importantly, ectopic expression of ALKBH5 partially rescued the phenotype caused by KDM4C KD (Figure 5L), indicating that ALKBH5 mediated the function of KDM4C in leukemia cells.

To investigate the underlying mechanism by which KDM4C regulates ALKBH5 expression, we performed ATAC-seq to assess the *cis*-regulatory landscape of KDM4C-KD leukemia cells. As shown in Figure 5M, KDM4C KD resulted in global loss of chromatin accessibility (Figures 5M and S5O). This observation is clearly illustrated by the region that surrounds the *ALKBH5* locus (Figures 5N and S5P). Furthermore, loss of KDM4C caused accumulation of repressive H3K9me3, with a concomitant reduction of transcriptional factor MYB and active RNA polymerase II-CTD (Pol II-CTD) binding (Figures 5O and S5Q). Together, these results indicate that KDM4C regulates *ALKBH5* expression in leukemia cells by increasing chromatin accessibility and promoting the binding of MYB and Pol II-CTD to the *ALKBH5* promoter.

ALKBH5 Regulates mRNA Stability by Altering m^{6}A Modification

To comprehensively understand the regulatory role of ALKBH5 in leukemogenesis, we conducted an RNA-seq assay and compared the gene expression profiles of leukemia cells following *ALKBH5* KD, with or without ALKBH5 restoration. A total of 399 genes were found to be differentially expressed by at least 2-fold (Figures 6A and S6A). The altered genes were closely related to amino acid metabolism, cell cycle G2-M regulation, PI3K/AKT signaling, apoptosis, and differentiation (Figures 6A–6D). Gene set enrichment analysis (GSEA) also showed the enrichment of differentiation-related genes in ALKBH5-KD cells (Figures 6B and S6B). Upon ALKBH5 deletion, there was an increase in the expression levels of the genes downregulated by HOXA9 and MEIS1 and the gene set downregulated in HSCs (Figures 6B and S6B). Additionally, an obvious enrichment for

Figure 4. Alkbh5 Is Dispensable for Normal Hematopoiesis and HSC Function

(A) CFU assay using cord blood-derived CD34$^+$ HSPCs from three individual units upon knockdown of ALKBH5.

(B) Blood count analysis in the PB of WT and *Alkbh5*$^{-/-}$ mice at 2 weeks after pIpC treatment (n = 4–6).

(C) Percentages of different lineage cells in the PB at 2 weeks after pIpC treatment (n = 11 for WT and *Alkbh5*$^{-/-}$).

(D–F) Percentages of different populations of mature lineage cells (D), progenitors (E), and stem cells (F) in the bone marrow of WT and *Alkbh5*$^{-/-}$ mice at 2 weeks after pIpC treatment (n = 6).

(G and H) Total cell numbers of different stem cell (G) and progenitor (H) populations in bone marrow at 2 weeks after pIpC treatment (n = 6 for WT and *Alkbh5*$^{-/-}$).

(I) CFU assay of Lin$^-$ bone marrow cells from WT and *Alkbh5*$^{-/-}$ mice at 2 weeks after pIpC treatment. Left: colony numbers; right: representative clone image.

(J) Competitive repopulation assay. Flow cytometry analysis for different donor-derived cell lineages in PB of recipient mice 4, 8, 12, and 16 weeks after BMT (n = 7–9).

(K and L) Percentage of donor-derived progenitor (K) and stem cell (L) compartments in the bone marrow of recipients 16 weeks after BMT.

(M) Secondary BMT showing comparable long-term function of WT and *Alkbh5*$^{-/-}$ HSCs. Flow cytometry analysis for different donor-derived cell lineages in PB of recipient mice 4, 6, 8, and 12 weeks after BMT (n = 5).

n.s., no significance; error bars denote mean ± SEM.

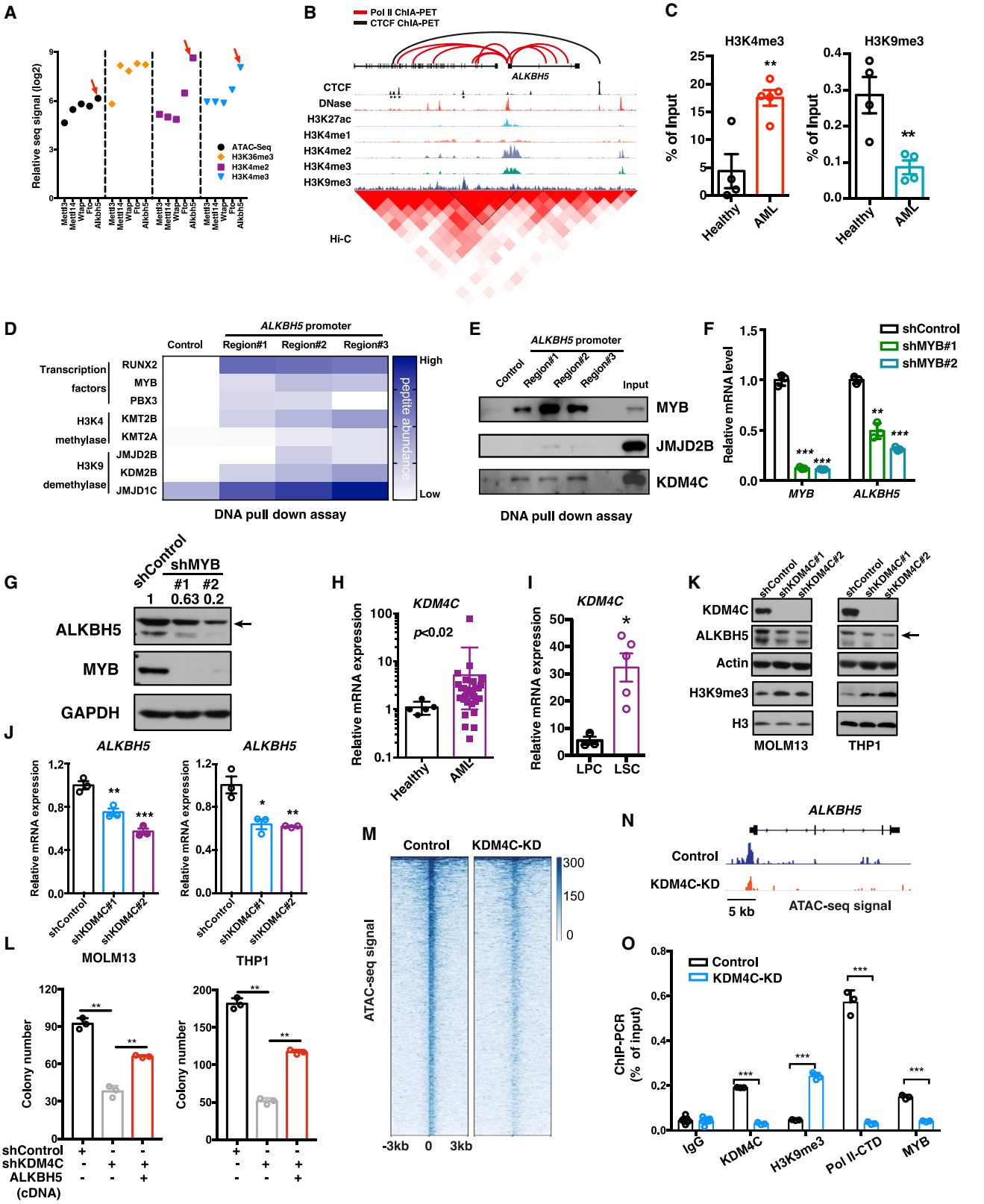

(legend on next page)

HSC signature was observed in AML patients with high ALKBH5 levels (Figure S6C).

To test whether the altered gene expression could be a consequence of ALKBH5-medidated m^{6}A demethylation, we mapped the m^{6}A methylomes by m^{6}A sequencing. In line with a previous analysis, m^{6}A sites were primarily found in both exons and 3′ UTR, and the most m^{6}A-enriched sites were located near the stop codon, displaying the canonical m^{6}A motif, DRACH (Figure S6D). Although ALKBH5 KD did not severely affect the m^{6}A distribution in genomic regions, and the frequency of m^{6}A sites per mRNA ranged from one to five or more m^{6}A sites per gene, ALKBH5 KD caused a significant increase in the total number of m^{6}A peaks (Figures S6E and S6F). Remarkably, up to 2,151 transcripts showed elevated m^{6}A enrichment, while 506 decreased transcripts were also present, which could not directly be targets, considering the demethylase activity of ALKBH5 (Figure 6E). By integrating transcriptome and m^{6}A methylomes analysis, we found that 1,594 mRNA transcripts with hyper-methylated m^{6}A peaks were significantly downregulated following ALKBH5 KD compared with control cells, which occupied 74% of the 2,151 hyper-methylated m^{6}A peaks. The remaining 557 mRNA transcripts with m^{6}A modification were upregulated upon ALKBH5 deletion (Figure 6F). Notably, when restored, 1,778 hypo-methylated m^{6}A peaks were identified, with 43% of these m^{6}A-marked transcripts upregulated and 57% downregulated (Figure 6F). The change in the expression levels of m^{6}A-marked transcripts may arise from alterations in their half-life. Therefore, we measured the transcriptome-wide mRNA decay rate in leukemia cells using thiol-linked alkylation for the metabolic sequencing of RNA (SLAM-seq) (Herzog et al., 2017). In line with a previous study (Zheng et al., 2013), we observed slightly reduced global mRNA stability in ALKBH5-KD cells (Figure 6G). Among these transcripts, we further confirmed that mRNA stabilities of differentiation-related genes, such as *ID1*, *ID2*, and *ID3*, were significantly increased upon ALKBH5 KD, but ALKBH5 deletion decreased mRNA stabilities of genes involved in serine biosynthesis, including *PHGDH* and *PSAT1*. These effects can be rescued upon restoration of ALBKH5 (Figures 6H and 6I). In addition, ectopic expression of PHGDH functionally rescued the clonogenic defects caused by ALKBH5 KD in leukemia cells (Figure 6J). As m^{6}A modification also affects translational efficiency (TE) (Wang et al., 2015), we further performed ribosome profiling (RIBO-seq) to measure the TE. Interestingly, ALKBH5 KD did not significantly alter the global TE of m^{6}A or non-m^{6}A-marked mRNA (Figures 6K and S6G). The outcomes of mRNA m^{6}A modification are executed by different m^{6}A readers (Shi et al., 2019). YTHDF2 is the major m^{6}A reader that promotes degradation of its target transcripts, whereas IGF2BP1/2/3 stabilize m^{6}A-marked mRNA. Therefore, we knocked down these readers in ALKBH5-KD leukemia cells and observed the restoration of *PHGDH*, *ID2*, and *ID3* expression along with deficiency of YTHDF2 or IGF2BP1/2 (Figures S6H and S6I), suggesting that YTHDF2 and IGF2BPs are the m^{6}A readers for *PHGDH* and *ID2/3*, respectively. Together, these results suggest that ALKBH5 regulates mRNA stabilities of its targets in AML cells by altering their m^{6}A modification.

ALKBH5 Regulates *AXL* mRNA Stability in Leukemia Cells

Interestingly, we observed strong enrichment of the gene sets of the PI3K/AKT/mTOR and protein Ser/Thr phosphatase activity pathways in ALKBH5^{high} cases from three AML patient cohorts (Figures 7A–7C), suggesting that ALKBH5 affects kinase phosphorylation pathways. We found that ALKBH5 KD markedly downregulated expression of *AXL*, accompanied by increased m^{6}A levels in its 3′ UTR (Figure 7D). AXL belongs to the receptor tyrosine kinase (RTK) TYRO3, AXL, and MERTK (TAM) family and is constitutively active in multiple types of cancer, including AML (Park et al., 2013, 2015; Rochlitz et al., 1999). Activation of TAM RTKs results in stimulation of a range of pathways, including PI3K/AKT/mTOR. As expected, downregulation of AXL caused by ALKBH5 KD reduced the activation of downstream kinase signaling, including p-SRC, p-AKT, p-ERK1/2, p-STAT3, and p-PLCγ, which were rescued upon restoration of ALKBH5 expression (Figures 7E and S7A). Therefore, we decided to further explore the detailed mechanism by which ALKBH5 regulates AXL expression. Consistent with our sequencing data

Figure 5. KDM4C Regulates ALKBH5 Expression by Modulating Chromatin Accessibility

(A) Integrated analysis of histone modifications and chromatin accessibility of m^{6}A modifiers in murine leukemia cells (datasets from GSE61022 and GSE60193).
(B) Comprehensive analysis of the *ALKBH5* locus in K562 cells (datasets from ENCODE).
(C) ChIP-qPCR analysis of H3K4me3 and H3K9me3 enrichment in the *ALKBH5* protomer in AML patient-derived leukemia cells. Each dot represents one individual sample.
(D) Heatmap of DNA pull-down in combination with mass spectrometry assay showing enrichment of transcription factors (RUNX2, MYB, and PBX3), H3K4 methylases (KMT2A and KMT2B), and H3K9 demethylase (JMJD2B, KDM2B, and JMJD1C) in the *ALKBH5* promoter.
(E) Immunoblot validation of DNA pull-down assay showing the binding of MYB, JMJD2B, and KDM4C to the *ALKBH5* promoter.
(F) qRT-PCR analysis showing *ALKBH5* and *MYB* expression in leukemia cells transduced with shRNAs targeting *MYB*.
(G) Immunoblot showing protein expression of ALKBH5 and MYB in leukemia cells after MYB knockdown.
(H) qRT-PCR analysis showing higher expression of *KDM4C* in AML patient-derived primary leukemia cells (n = 28) than in normal bone marrow (BM) cells from healthy donors (n = 5).
(I) *KDM4C* expression in LPCs (n = 3) and LSCs (n = 5) from GSE34044.
(J) qRT-PCR analysis of *ALKBH5* expression after KDM4C knockdown.
(K) Immunoblotting for KDM4C, ALKBH5, and H3K9me3. H3 and actin were used as loading control.
(L) CFU assay showing the rescue of phenotype by re-expressing ALKBH5 in KDM4C-KD cells.
(M) Heatmap showing the ATAC-seq signal at TSSs ± 3 kb regions for all genes in MOLM-13 cells transduced with shcontrol or sh*KDM4C*.
(N) Representative integrative genomics viewer (IGV) displaying the ATAC-seq signal of *ALKBH5* locus in MOLM-13 cells transduced with shcontrol or sh*KDM4C*.
(O) ChIP-qPCR analysis of KDM4C, Pol II-CTD, and H3K9me3 enrichment in the *ALKBH5* protomer in MOLM-13 cells transduced with shcontrol or sh*KDM4C*.
One representative result of two independent experiments is shown.
**$p < 0.01$ and ***$p < 0.001$ (t test). Error bars denote mean ± SEM.

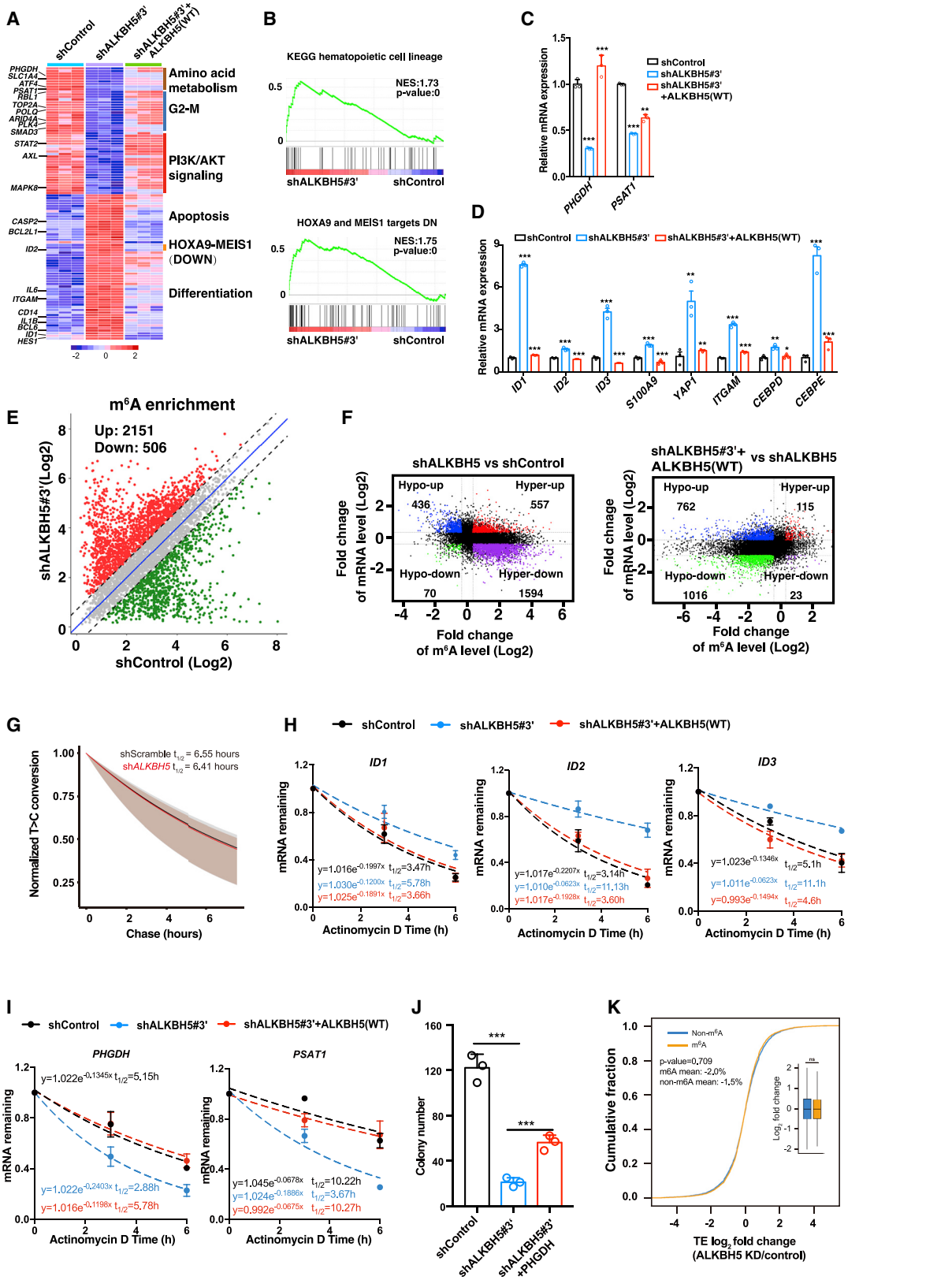

(legend on next page)

(Figure 7D), we confirmed the decreased mRNA level of *AXL* following ALKBH5 deletion, which was reversed upon restoring ALKBH5 expression (Figures 7F and S7B). Moreover, deficiency of *Alkbh5* resulted in downregulation of *Axl* in a dose-dependent manner in leukemia cells and caused obvious downregulation of *Axl* in LICs from AML mice (Figures 7G and S7C). Similarly, downregulation of *Phgdh* and *Psat1* was also observed in primary *Alkbh5*$^{-/-}$ leukemia cells and LICs (Figure S7D). Using m^{6}A gene-specific qRT-PCR, we found that the levels of m^{6}A were increased upon ALKBH5 KD in the *AXL* transcript, which was rescued following ALKBH5 restoration (Figures 7H and S7E). Consistently, forced expression of WT ALKBH5, but not the mutant ALKBH5, substantially restored expression of AXL upon KD of ALKBH5 in leukemia cells (Figure S7F). We next asked whether ALKBH5 directly binds *AXL* transcripts by performing ALKBH5 RIP-PCR. We observed significant enrichment of *AXL* transcripts in m^{6}A region, indicating that ALKBH5 directly binds *AXL* transcripts in an m^{6}A-dependent manner (Figure 7I). Using luciferase reporter assay, we found that ALKBH5 KD decreased the activity of the luciferase construct containing *AXL* 3′ UTR (Figure 7J). To investigate whether ALKBH5 regulates *AXL* expression by modulating its mRNA stability, we treated control or ALBKH5-KD MOLM-13 cells with the transcription inhibitor actinomycin D (Act D) and measured the half-life of the *AXL* transcripts. Indeed, ALKBH5 KD caused a noticeable decrease in the half-life of *AXL* (Figure 7K). Similar effects were also found in primary *Alkbh5*$^{-/-}$ leukemia cells (Figure 7L). We further explored the underlying mechanism for this. KD of YTHDF2 obviously restored *AXL* mRNA level in ALKBH5-deficient leukemia cells (Figure 7M), indicating that YTHDF2 is the m^{6}A reader for *AXL* mRNA. Together, these findings suggest that ALKBH5 regulates *AXL* stability in leukemia cells in an m^{6}A-dependent manner, which is mediated by YTHDF2.

Next, we proposed that to a certain extent, AXL mediates the function of ALBKH5 in leukemia cells. Similarly, KD of AXL inhibited the cellular growth and clonogenic potential of leukemia cells, which recapitulated the phenotype resulting from ALKBH5 KD (Figures S7G–S7J). Therefore, we re-expressed AXL in ALKBH5-KD leukemia cells and primary murine LICs and found that the ectopic expression of AXL partially rescued the clonogenic defect resulting from ALKBH5 deficiency (Figures 7N, 7O, and S7K). Overall, these data indicate that AXL is a functional downstream target of ALKBH5.

DISCUSSION

Here we show that ALKBH5 is selectively required for AML development and maintenance of LSC function, but not for normal hematopoiesis (Figure 7P). Complementary findings are also reported by Shen et al., 2020 (in this issue of *Cell Stem Cell*). These findings provide a rationale for specifically eradicating AML LSCs, but not their normal counterparts, by targeting ALKBH5. This is especially important considering the broader function of m^{6}A modification and its related modifiers in various biological processes.

Our study demonstrates that chromatin state alterations during leukemogenesis regulate ALKBH5 expression. To our knowledge, this is the first established link between epigenetic change and m^{6}A modification. Previous studies have revealed the critical function of H3K9me3 in cancer (Schuster-Böckler and Lehner, 2012), but the related gene loci were not well defined. Our findings indicate that ALKBH5 is one of the related loci affected by H3K9me3 in leukemogenesis, and KDM4C removes the H3K9me3 marks on *ALKBH5* locus. MYB is essential for normal hematopoiesis, as well as AML initiation and maintenance (Lieu and Reddy, 2009; Ramsay and Gonda, 2008), and its expression is regulated by METTL14 through m^{6}A-based post-transcriptional regulation (Weng et al., 2018). Surprisingly, we found that MYB acts as one of the upstream transcriptional factors for ALKBH5 and positively regulates its expression.

Our findings reveal the crucial role of ALKBH5 in specifically regulating the function of AML LSCs, which establishes the rationale for selectively targeting AML LSCs using ALKBH5 as a therapeutic target. FTO, another m^{6}A demethylase, plays a critical oncogenic role in certain subtypes of AML (Li et al., 2017b). Interestingly, upon FTO and ALKBH5 KD, fewer than 10% the affected transcripts were overlapped (data not shown), suggesting that they have different downstream targets. Also, the distinct consequences of m^{6}A removal by ALKBH5 might result from different effects of m^{6}A modification on different transcripts mediated by m^{6}A readers (Yang et al., 2018). Moreover, global mRNA stability and TE were not significantly changed upon ALKBH5 deficiency, which implies that ALKBH5 may affect the specific targets or pathways. Given that the m^{6}A readers YTHDF2 and IGF2BPs are important for mediating the effect of ALKBH5 on some of its targets, it will be important to further elucidate the underlying mechanisms in the future.

Figure 6. ALKBH5 Regulates mRNA Stability by Altering m^{6}A Modification

(A) Heatmap showing differential expression of ALKBH5 targets in leukemia cells transduced with indicated lentivirus.

(B) GSEA plot showing enrichment of gene sets of hematopoietic differentiation and downregulated targets of HOXA9 and MEIS1 in ALKBH5-KD leukemia cells.

(C) qRT-PCR validation of the effect of ALKBH5 on the expression levels of *PHGDH* and *PSAT1* in leukemia cells transduced with indicated lentivirus.

(D) qRT-PCR validation of the effect of ALKBH5 on the expression levels of *ID1*, *ID2*, *ID3*, *S100A9*, *YAP1*, *ITGAM*, *CEBPD*, and *CEBPE* in leukemia cells transduced with indicated lentivirus.

(E) Scatterplot showing m^{6}A enrichment on mRNAs of leukemia cells transduced with shControl and shALKBH5.

(F) Distribution of genes with a significant change in both m^{6}A level and overall transcript level in ALKBH5-KD cells versus control cells and in ALKBH5-rescued versus ALKBH5-KD cells.

(G) SLAM-seq analysis showing the cumulative distributions of transcript half-life in leukemia cells with or without knockdown of ALKBH5.

(H) The mRNA half-life ($t_{1/2}$) of *ID1*, *ID2*, and *ID3* in leukemia cells transduced with the indicated lentivirus.

(I) The mRNA half-life ($t_{1/2}$) of *PHGDH* and *PSAT1* in leukemia cells transduced with the indicated lentivirus.

(J) CFU assay for PHGDH functional rescue of the clonogenic defects of ALKBH5-KD leukemia cells.

(K) RIBO-seq analysis showing the comparable TE of leukemia cells with or without knockdown of ALKBH5. Inset: boxplot showing fold change (shALKBH5 versus shControl) in TE of non-m^{6}A or m^{6}A transcripts.

*$p < 0.05$, **$p < 0.01$, and ***$p < 0.001$ (t test). Error bars denote mean ± SEM.

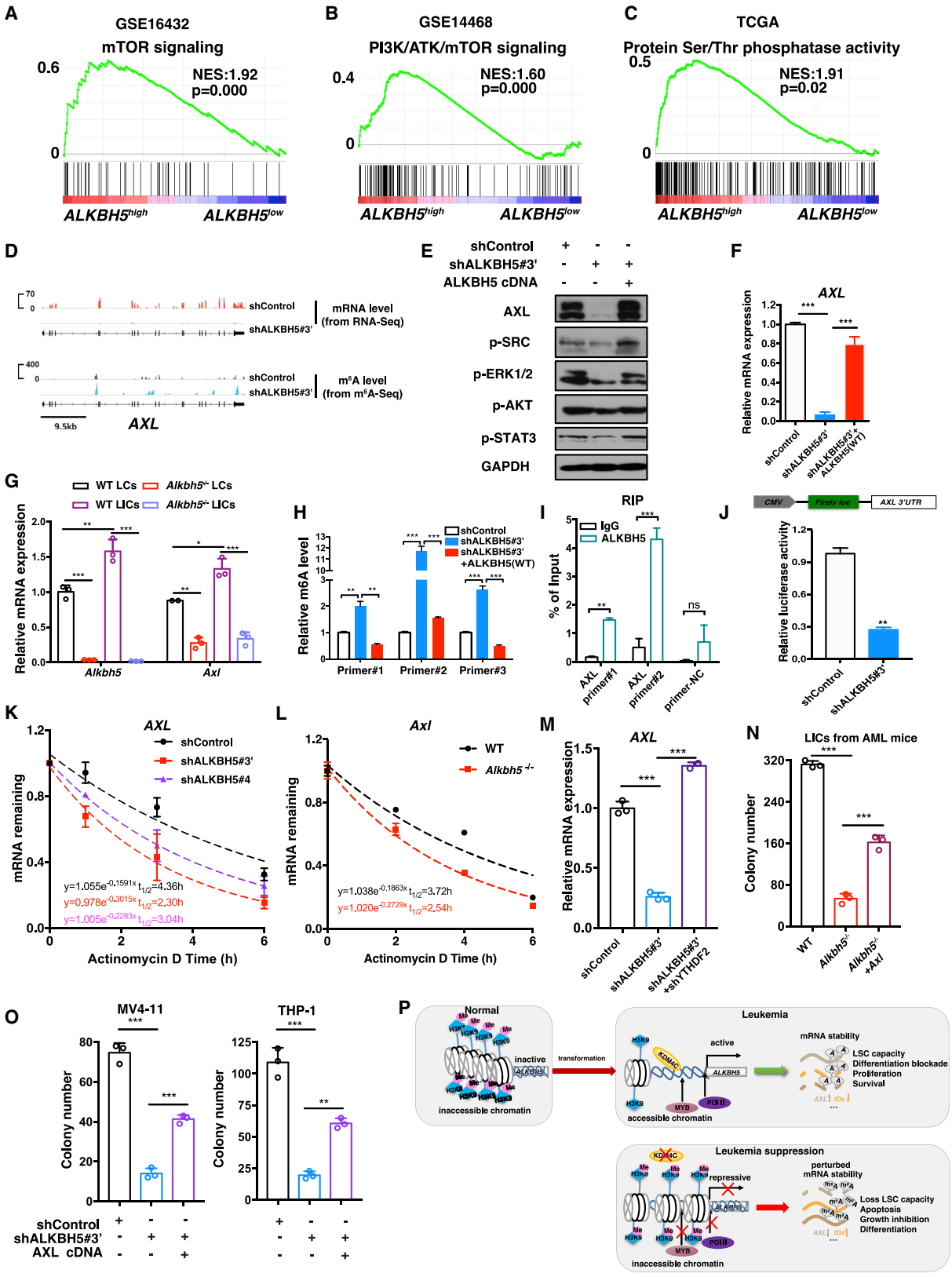

(legend on next page)

Activation of AXL stimulates PI3K, MAPK, JAK/STAT, and NF-κB signaling and is associated with AML chemoresistance (Graham et al., 2014; Hong et al., 2008). Our study identified that ALKBH5 regulated the PI3K/AKT pathway by modulating *AXL* mRNA stability. Moreover, we showed that elevated ALKBH5 expression correlated with poor prognosis in AML patients. These findings might connect m^{6}A modification with AML chemoresistance, which is supported by a recent study showing the involvement of FTO in acquired resistance to tyrosine kinase inhibitors (Yan et al., 2018). Collectively, our results provide mechanistic insights into how expression of m^{6}A modifiers is regulated in AML leukemogenesis and suggest a potential therapeutic strategy for selectively treating AML by targeting ALKBH5.

STAR★METHODS

Detailed methods are provided in the online version of this paper and include the following:

- KEY RESOURCES TABLE
- RESOURCE AVAILABILITY
  - Lead Contact
  - Materials Availability
  - Data and Code Availability
- EXPERIMENTAL MODEL AND SUBJECT DETAILS
  - Mice
  - Primary AML patient and cord blood samples
  - Cell lines
  - Primary cell culture
- METHOD DETAILS
  - Plasmids and lentivirus production
  - Cell proliferation and *in vitro* colony-forming assay
  - m^{6}A dot blot and quantification assay
  - Generation and analysis of murine MLL-AF9 leukemia model
  - *In Vivo* Xenograft Assay
  - Competitive repopulation assay
  - Flow cytometry analysis and cell sorting
  - DNA pull-down assay
  - Mass Spectrometry
  - ATAC-sequencing
  - RNA-seq and m^{6}A-seq and data analysis
  - SLAM-seq and data analysis
  - RIBO-seq and data analysis
  - Public database analysis
  - Luciferase reporter assay
  - RNA decay assay
  - Quantitative RT-PCR
  - Chromatin immunoprecipitation (ChIP)-qPCR assays
  - RIP-PCR
  - Western blot analysis
- QUANTIFICATION AND STATISTICAL ANALYSIS

SUPPLEMENTAL INFORMATION

Supplemental Information can be found online at https://doi.org/10.1016/j.stem.2020.04.001.

ACKNOWLEDGMENTS

We acknowledge the members of our laboratory for helpful discussions. This work is supported by grants to H.Z. from the National Key Research and Development Program of China (2017YFA0505600), the National Natural Science Foundation of China (81722003, 81870124), the Wuhan Science and Technology Program for Application and Basic Research Project (2018060401011325), the Natural Science Foundation of Hubei Province (2019CFA073), and the Hubei Provincial Natural Science Foundation for Creative Research Group (2018CFA018). This work was also supported by grants from the National Natural Science Foundation of China (81500133 to L.Li.).

AUTHOR CONTRIBUTIONS

Jiazhen Wang and H.Z. conceived the project. Jiazhen Wang, Yicun Li., P.W., G.H., and H.Z. designed the experiments and analyzed the data. Yicun Li and Jiwei Chang. performed bioinformatic analyses with conceptual input from Jiazhen Wang and H.Z.. Jiazhen Wang and P.W. performed *in vitro* function and mechanisms studies. Jiazhen Wang and G.H. performed xenograft and knockout mouse model studies, respectively. Other researchers in the lab (Jin Wen, Yashu Li, Jihua Chai, T.Z., R.Y., Y.S., X.X., M.F., Q.W., J.H., Y.C., T.Z., Z.G., C.G., J.L., M.C., K.G., and W.L.) helped with experiments. H.C., L. Li, F.Z., L. Liu, and Y. Luo provided AML samples and clinical data. S.L. helped advise this study. H.Z. supervised the project. Jiazhen Wang, Yicun Li., P.W., G.H., and H.Z. wrote the manuscript.

DECLARATION OF INTERESTS

The authors declare no competing interests.

Figure 7. ALKBH5 Regulates the Stability of *AXL* in an m^{6}A-Dependent Manner Mediated by YTHDF2

(A–C) GSEA plot showing enrichment of gene sets for mTOR signaling, PI3K/AKT/mTOR signaling, and porotein Ser/Thr phosphatase activity pathways in ALKBH5^{high} versus ALKBH5^{low} groups from different AML patient cohorts GSE16432 (A), GSE14468 (B), and The Cancer Genome Atlas (TCGA) (C), respectively.
(D) IGV tracks displaying mRNA and m^{6}A abundances of *AXL* transcript in ALKBH5-KD and control cells.
(E) Immunoblot for AXL, p-SRC, p-ERK1/2, p-AKT, and p-STAT3 in THP1 cells 4 days after transduction with the indicated constructs (GAPDH as loading control).
(F) qRT-PCR analysis showing *AXL* levels in THP1 leukemia cells.
(G) qRT-PCR analysis showing *Alkbh5* and *Axl* levels in leukemia cells and LICs from WT and *Alkbh5*$^{-/-}$ AML mice.
(H) m^{6}A-RIP-qPCR analysis of m^{6}A enrichment on *AXL* mRNA in leukemia cells.
(I) RIP-qPCR analysis of ALKBH5 binding to *AXL* mRNA in leukemia cells. Primers 1 and 2 locate 3′ UTR around m^{6}A sites and primer NC in the distal region without m^{6}A site.
(J) Relative activity of *AXL* 3′ UTR firefly Luciferase reporter in 293T cells treated with control or ALKBH5 shRNAs.
(K) The mRNA half-life ($t_{1/2}$) of *AXL* in MOLM-13 cells transduced with shALKBH5.
(L) The mRNA half-life ($t_{1/2}$) of *Axl* in WT and *Alkbh5*$^{-/-}$ LICs.
(M) qRT-PCR analysis showing restoration of *AXL* mRNA expression in ALKBH5-KD THP1 cells upon knockdown of YTHDF2.
(N) CFU assay of LICs from WT and *Alkbh5*$^{-/-}$ AML mice.
(O) CFU assay of MV4-11 and THP1 cells after transduction with indicated lentiviruses.
(P) Working model showing the role of ALKBH5 in leukemia.
**p < 0.01 and ***p < 0.001 (t test). Error bars, mean ± SEM.

Received: July 12, 2019
Revised: February 13, 2020
Accepted: March 31, 2020
Published: May 12, 2020

REFERENCES

Barbieri, I., Tzelepis, K., Pandolfini, L., Shi, J., Millán-Zambrano, G., Robson, S.C., Aspris, D., Migliori, V., Bannister, A.J., Han, N., et al. (2017). Promoter-bound METTL3 maintains myeloid leukaemia by m^6A-dependent translation control. Nature *552*, 126–131.

Chen, C.Y., Ezzeddine, N., and Shyu, A.B. (2008). Messenger RNA half-life measurements in mammalian cells. Methods Enzymol. *448*, 335–357.

Chen, C.W., Koche, R.P., Sinha, A.U., Deshpande, A.J., Zhu, N., Eng, R., Doench, J.G., Xu, H., Chu, S.H., Qi, J., et al. (2015). DOT1L inhibits SIRT1-mediated epigenetic silencing to maintain leukemic gene expression in MLL-rearranged leukemia. Nat. Med. *21*, 335–343.

Cheung, N., Fung, T.K., Zeisig, B.B., Holmes, K., Rane, J.K., Mowen, K.A., Finn, M.G., Lenhard, B., Chan, L.C., and So, C.W. (2016). Targeting aberrant epigenetic networks mediated by PRMT1 and KDM4C in acute myeloid leukemia. Cancer Cell *29*, 32–48.

Chi, P., Allis, C.D., and Wang, G.G. (2010). Covalent histone modifications–miswritten, misinterpreted and mis-erased in human cancers. Nat. Rev. Cancer *10*, 457–469.

ENCODE Project Consortium (2012). An integrated encyclopedia of DNA elements in the human genome. Nature *489*, 57–74.

Corces, M.R., Buenrostro, J.D., Wu, B., Greenside, P.G., Chan, S.M., Koenig, J.L., Snyder, M.P., Pritchard, J.K., Kundaje, A., Greenleaf, W.J., et al. (2016). Lineage-specific and single-cell chromatin accessibility charts human hematopoiesis and leukemia evolution. Nat. Genet. *48*, 1193–1203.

Cui, Q., Shi, H., Ye, P., Li, L., Qu, Q., Sun, G., Sun, G., Lu, Z., Huang, Y., Yang, C.G., et al. (2017). m^6A RNA methylation regulates the self-renewal and tumorigenesis of glioblastoma stem cells. Cell Rep. *18*, 2622–2634.

Cusanovich, D.A., Hill, A.J., Aghamirzaie, D., Daza, R.M., Pliner, H.A., Berletch, J.B., Filippova, G.N., Huang, X., Christiansen, L., DeWitt, W.S., et al. (2018). A single-cell atlas of in vivo mammalian chromatin accessibility. Cell *174*, 1309–1324.e18.

Desrosiers, R., Friderici, K., and Rottman, F. (1974). Identification of methylated nucleosides in messenger RNA from Novikoff hepatoma cells. Proc. Natl. Acad. Sci. U S A *71*, 3971–3975.

Döhner, H., Weisdorf, D.J., and Bloomfield, C.D. (2015). Acute myeloid leukemia. N. Engl. J. Med. *373*, 1136–1152.

Dolnik, A., Engelmann, J.C., Scharfenberger-Schmeer, M., Mauch, J., Kelkenberg-Schade, S., Haldemann, B., Fries, T., Krönke, J., Kühn, M.W., Paschka, P., et al. (2012). Commonly altered genomic regions in acute myeloid leukemia are enriched for somatic mutations involved in chromatin remodeling and splicing. Blood *120*, e83–e92.

Dominissini, D., Moshitch-Moshkovitz, S., Schwartz, S., Salmon-Divon, M., Ungar, L., Osenberg, S., Cesarkas, K., Jacob-Hirsch, J., Amariglio, N., Kupiec, M., et al. (2012). Topology of the human and mouse m^6A RNA methylomes revealed by m^6A-seq. Nature *485*, 201–206.

Eppert, K., Takenaka, K., Lechman, E.R., Waldron, L., Nilsson, B., van Galen, P., Metzeler, K.H., Poeppl, A., Ling, V., Beyene, J., et al. (2011). Stem cell gene expression programs influence clinical outcome in human leukemia. Nat. Med. *17*, 1086–1093.

Garraway, L.A., and Lander, E.S. (2013). Lessons from the cancer genome. Cell *153*, 17–37.

Graham, D.K., DeRyckere, D., Davies, K.D., and Earp, H.S. (2014). The TAM family: phosphatidylserine sensing receptor tyrosine kinases gone awry in cancer. Nat. Rev. Cancer *14*, 769–785.

Han, D., Liu, J., Chen, C., Dong, L., Liu, Y., Chang, R., Huang, X., Liu, Y., Wang, J., Dougherty, U., et al. (2019). Anti-tumour immunity controlled through mRNA m^6A methylation and YTHDF1 in dendritic cells. Nature *566*, 270–274.

Herzog, V.A., Reichholf, B., Neumann, T., Rescheneder, P., Bhat, P., Burkard, T.R., Wlotzka, W., von Haeseler, A., Zuber, J., and Ameres, S.L. (2017). Thiol-linked alkylation of RNA to assess expression dynamics. Nat. Methods *14*, 1198–1204.

Hong, C.C., Lay, J.D., Huang, J.S., Cheng, A.L., Tang, J.L., Lin, M.T., Lai, G.M., and Chuang, S.E. (2008). Receptor tyrosine kinase AXL is induced by chemotherapy drugs and overexpression of AXL confers drug resistance in acute myeloid leukemia. Cancer Lett. *268*, 314–324.

Huang, D.W., Sherman, B.T., and Lempicki, R.A. (2009). Systematic and integrative analysis of large gene lists using DAVID bioinformatics resources. Nat. Protoc. *4*, 44–57.

Jia, G., Fu, Y., Zhao, X., Dai, Q., Zheng, G., Yang, Y., Yi, C., Lindahl, T., Pan, T., Yang, Y.G., and He, C. (2011). N^6-methyladenosine in nuclear RNA is a major substrate of the obesity-associated FTO. Nat. Chem. Biol. *7*, 885–887.

Jing, D., Huang, Y., Liu, X., Sia, K.C.S., Zhang, J.C., Tai, X., Wang, M., Toscan, C.E., McCalmont, H., Evans, K., et al. (2018). Lymphocyte-specific chromatin accessibility pre-determines glucocorticoid resistance in acute lymphoblastic leukemia. Cancer Cell *34*, 906–921.e8.

Lara-Astiaso, D., Weiner, A., Lorenzo-Vivas, E., Zaretsky, I., Jaitin, D.A., David, E., Keren-Shaul, H., Mildner, A., Winter, D., Jung, S., et al. (2014). Immunogenetics. Chromatin state dynamics during blood formation. Science *345*, 943–949.

Ley, T.J., Miller, C., Ding, L., Raphael, B.J., Mungall, A.J., Robertson, A., Hoadley, K., Triche, T.J., Jr., Laird, P.W., Baty, J.D., et al.; Cancer Genome Atlas Research Network (2013). Genomic and epigenomic landscapes of adult de novo acute myeloid leukemia. N. Engl. J. Med. *368*, 2059–2074.

Li, H.B., Tong, J., Zhu, S., Batista, P.J., Duffy, E.E., Zhao, J., Bailis, W., Cao, G., Kroehling, L., Chen, Y., et al. (2017a). m^6A mRNA methylation controls T cell homeostasis by targeting the IL-7/STAT5/SOCS pathways. Nature *548*, 338–342.

Li, Z., Weng, H., Su, R., Weng, X., Zuo, Z., Li, C., Huang, H., Nachtergaele, S., Dong, L., Hu, C., et al. (2017b). FTO plays an oncogenic role in acute myeloid leukemia as a N^6-methyladenosine RNA demethylase. Cancer Cell *31*, 127–141.

Lieu, Y.K., and Reddy, E.P. (2009). Conditional c-myb knockout in adult hematopoietic stem cells leads to loss of self-renewal due to impaired proliferation and accelerated differentiation. Proc. Natl. Acad. Sci. U S A *106*, 21689–21694.

Liu, J., Yue, Y., Han, D., Wang, X., Fu, Y., Zhang, L., Jia, G., Yu, M., Lu, Z., Deng, X., et al. (2014). A METTL3-METTL14 complex mediates mammalian nuclear RNA N6-adenosine methylation. Nat. Chem. Biol. *10*, 93–95.

Mauer, J., Luo, X., Blanjoie, A., Jiao, X., Grozhik, A.V., Patil, D.P., Linder, B., Pickering, B.F., Vasseur, J.J., Chen, Q., et al. (2017). Reversible methylation of m^6A_m in the 5′ cap controls mRNA stability. Nature *541*, 371–375.

Meng, J., Lu, Z., Liu, H., Zhang, L., Zhang, S., Chen, Y., Rao, M.K., and Huang, Y. (2014). A protocol for RNA methylation differential analysis with MeRIP-Seq data and exomePeak R/Bioconductor package. Methods *69*, 274–281.

Meyer, K.D., and Jaffrey, S.R. (2014). The dynamic epitranscriptome: N^6-methyladenosine and gene expression control. Nat. Rev. Mol. Cell Biol. *15*, 313–326.

Meyer, K.D., Saletore, Y., Zumbo, P., Elemento, O., Mason, C.E., and Jaffrey, S.R. (2012). Comprehensive analysis of mRNA methylation reveals enrichment in 3′ UTRs and near stop codons. Cell *149*, 1635–1646.

Mootha, V.K., Lindgren, C.M., Eriksson, K.-F., Subramanian, A., Sihag, S., Lehar, J., Puigserver, P., Carlsson, E., Ridderstråle, M., Laurila, E., et al. (2003). PGC-1α-responsive genes involved in oxidative phosphorylation are coordinately downregulated in human diabetes. Nat. Genet. *34*, 267–273.

Park, I.K., Mishra, A., Chandler, J., Whitman, S.P., Marcucci, G., and Caligiuri, M.A. (2013). Inhibition of the receptor tyrosine kinase Axl impedes activation of the FLT3 internal tandem duplication in human acute myeloid leukemia: implications for Axl as a potential therapeutic target. Blood *121*, 2064–2073.

Park, I.K., Mundy-Bosse, B., Whitman, S.P., Zhang, X., Warner, S.L., Bearss, D.J., Blum, W., Marcucci, G., and Caligiuri, M.A. (2015). Receptor tyrosine

kinase Axl is required for resistance of leukemic cells to FLT3-targeted therapy in acute myeloid leukemia. Leukemia *29*, 2382–2389.

Ramsay, R.G., and Gonda, T.J. (2008). MYB function in normal and cancer cells. Nat. Rev. Cancer *8*, 523–534.

Reid, D.W., Shenolikar, S., and Nicchitta, C.V. (2015). Simple and inexpensive ribosome profiling analysis of mRNA translation. Methods *91*, 69–74.

Rochlitz, C., Lohri, A., Bacchi, M., Schmidt, M., Nagel, S., Fopp, M., Fey, M.F., Herrmann, R., and Neubauer, A. (1999). Axl expression is associated with adverse prognosis and with expression of Bcl-2 and CD34 in de novo acute myeloid leukemia (AML): results from a multicenter trial of the Swiss Group for Clinical Cancer Research (SAKK). Leukemia *13*, 1352–1358.

Sanjana, N.E., Shalem, O., and Zhang, F. (2014). Improved vectors and genome-wide libraries for CRISPR screening. Nat. Methods *11*, 783–784.

Schuster-Böckler, B., and Lehner, B. (2012). Chromatin organization is a major influence on regional mutation rates in human cancer cells. Nature *488*, 504–507.

Shi, H., Zhang, X., Weng, Y.L., Lu, Z., Liu, Y., Lu, Z., Li, J., Hao, P., Zhang, Y., Zhang, F., et al. (2018). m^{6}A facilitates hippocampus-dependent learning and memory through YTHDF1. Nature *563*, 249–253.

Shen, C., Sheng, Y., Zhu, A., Robinson, S., Jiang, X., Dong, L., Chen, H., Su, R., Yin, Z., Li, W., et al. (2020). RNA demethylase ALKBH5 selectively promotes tumorigenesis and cancer stem cell self-renewal in acute myeloid leukemia. Cell Stem Cell *27*, this issue, 64–80.

Shi, H., Wei, J., and He, C. (2019). Where, when, and how: context-dependent functions of RNA methylation writers, readers, and erasers. Mol. Cell *74*, 640–650.

Shlush, L.I., Zandi, S., Mitchell, A., Chen, W.C., Brandwein, J.M., Gupta, V., Kennedy, J.A., Schimmer, A.D., Schuh, A.C., Yee, K.W., et al.; HALT Pan-Leukemia Gene Panel Consortium (2014). Identification of pre-leukaemic haematopoietic stem cells in acute leukaemia. Nature *506*, 328–333.

Shlush, L.I., Mitchell, A., Heisler, L., Abelson, S., Ng, S.W.K., Trotman-Grant, A., Medeiros, J.J.F., Rao-Bhatia, A., Jaciw-Zurakowsky, I., Marke, R., et al. (2017). Tracing the origins of relapse in acute myeloid leukaemia to stem cells. Nature *547*, 104–108.

Stewart, S.A., Dykxhoorn, D.M., Palliser, D., Mizuno, H., Yu, E.Y., An, D.S., Sabatini, D.M., Chen, I.S., Hahn, W.C., Sharp, P.A., et al. (2003). Lentivirus-delivered stable gene silencing by RNAi in primary cells. RNA *9*, 493–501.

Subramanian, A., Tamayo, P., Mootha, V.K., Mukherjee, S., Ebert, B.L., Gillette, M.A., Paulovich, A., Pomeroy, S.L., Golub, T.R., Lander, E.S., and Mesirov, J.P. (2005). Gene set enrichment analysis: a knowledge-based approach for interpreting genome-wide expression profiles. Proc. Natl. Acad. Sci. U S A *102*, 15545–15550.

Tessarz, P., and Kouzarides, T. (2014). Histone core modifications regulating nucleosome structure and dynamics. Nat. Rev. Mol. Cell Biol. *15*, 703–708.

van Galen, P., Hovestadt, V., Wadsworth Ii, M.H., Hughes, T.K., Griffin, G.K., Battaglia, S., Verga, J.A., Stephansky, J., Pastika, T.J., Lombardi Story, J., et al. (2019). Single-cell RNA-seq reveals AML hierarchies relevant to disease progression and immunity. Cell *176*, 1265–1281.e24.

Vu, L.P., Pickering, B.F., Cheng, Y., Zaccara, S., Nguyen, D., Minuesa, G., Chou, T., Chow, A., Saletore, Y., MacKay, M., et al. (2017a). The N^6-methyladenosine (m^{6}A)-forming enzyme METTL3 controls myeloid differentiation of normal hematopoietic and leukemia cells. Nat. Med. *23*, 1369–1376.

Vu, L.P., Prieto, C., Amin, E.M., Chhangawala, S., Krivtsov, A., Calvo-Vidal, M.N., Chou, T., Chow, A., Minuesa, G., Park, S.M., et al. (2017b). Functional screen of MSI2 interactors identifies an essential role for SYNCRIP in myeloid leukemia stem cells. Nat. Genet. *49*, 866–875.

Wang, X., Zhao, B.S., Roundtree, I.A., Lu, Z., Han, D., Ma, H., Weng, X., Chen, K., Shi, H., and He, C. (2015). N(6)-methyladenosine modulates messenger RNA translation efficiency. Cell *161*, 1388–1399.

Wang, Y., Song, F., Zhang, B., Zhang, L., Xu, J., Kuang, D., Li, D., Choudhary, M.N.K., Li, Y., Hu, M., et al. (2018). The 3D Genome Browser: a web-based browser for visualizing 3D genome organization and long-range chromatin interactions. Genome Biol. *19*, 151.

Wang, E., Lu, S.X., Pastore, A., Chen, X., Imig, J., Chun-Wei Lee, S., Hockemeyer, K., Ghebrechristos, Y.E., Yoshimi, A., Inoue, D., et al. (2019). Targeting an RNA-binding protein network in acute myeloid leukemia. Cancer Cell *35*, 369–384.e7.

Weng, H., Huang, H., Wu, H., Qin, X., Zhao, B.S., Dong, L., Shi, H., Skibbe, J., Shen, C., Hu, C., et al. (2018). METTL14 inhibits hematopoietic stem/progenitor differentiation and promotes leukemogenesis via mRNA m^{6}A modification. Cell Stem Cell *22*, 191–205.e9.

Winkler, R., Gillis, E., Lasman, L., Safra, M., Geula, S., Soyris, C., Nachshon, A., Tai-Schmiedel, J., Friedman, N., Le-Trilling, V.T.K., et al. (2019). m^{6}A modification controls the innate immune response to infection by targeting type I interferons. Nat. Immunol. *20*, 173–182.

Wong, S.H., Goode, D.L., Iwasaki, M., Wei, M.C., Kuo, H.P., Zhu, L., Schneidawind, D., Duque-Afonso, J., Weng, Z., and Cleary, M.L. (2015). The H3K4-methyl epigenome regulates leukemia stem cell oncogenic potential. Cancer Cell *28*, 198–209.

Xiang, Y., Laurent, B., Hsu, C.H., Nachtergaele, S., Lu, Z., Sheng, W., Xu, C., Chen, H., Ouyang, J., Wang, S., et al. (2017). RNA m^{6}A methylation regulates the ultraviolet-induced DNA damage response. Nature *543*, 573–576.

Yan, F., Al-Kali, A., Zhang, Z., Liu, J., Pang, J., Zhao, N., He, C., Litzow, M.R., and Liu, S. (2018). A dynamic N^6-methyladenosine methylome regulates intrinsic and acquired resistance to tyrosine kinase inhibitors. Cell Res. *28*, 1062–1076.

Yang, Y., Hsu, P.J., Chen, Y.S., and Yang, Y.G. (2018). Dynamic transcriptomic m^{6}A decoration: writers, erasers, readers and functions in RNA metabolism. Cell Res. *28*, 616–624.

Yoshida, H., Lareau, C.A., Ramirez, R.N., Rose, S.A., Maier, B., Wroblewska, A., Desland, F., Chudnovskiy, A., Mortha, A., Dominguez, C., et al. (2019). The *cis*-regulatory atlas of the mouse immune system. Cell *176*, 897–912.e20.

Yu, G., Wang, L.G., Han, Y., and He, Q.Y. (2012). clusterProfiler: an R package for comparing biological themes among gene clusters. OMICS *16*, 284–287.

Zhang, S., Zhao, B.S., Zhou, A., Lin, K., Zheng, S., Lu, Z., Chen, Y., Sulman, E.P., Xie, K., Bogler, O., et al. (2017). m^{6}A demethylase ALKBH5 maintains tumorigenicity of glioblastoma stem-like cells by sustaining FOXM1 expression and cell proliferation program. Cancer Cell *31*, 591–606.e6.

Zhang, Y., Xia, F., Liu, X., Yu, Z., Xie, L., Liu, L., Chen, C., Jiang, H., Hao, X., He, X., et al. (2018). JAM3 maintains leukemia-initiating cell self-renewal through LRP5/AKT/β-catenin/CCND1 signaling. J. Clin. Invest. *128*, 1737–1751.

Zheng, G., Dahl, J.A., Niu, Y., Fedorcsak, P., Huang, C.M., Li, C.J., Vågbø, C.B., Shi, Y., Wang, W.L., Song, S.H., et al. (2013). ALKBH5 is a mammalian RNA demethylase that impacts RNA metabolism and mouse fertility. Mol. Cell *49*, 18–29.

Zhou, J., Wan, J., Gao, X., Zhang, X., Jaffrey, S.R., and Qian, S.B. (2015). Dynamic m^{6}A mRNA methylation directs translational control of heat shock response. Nature *526*, 591–594.

STAR★METHODS

KEY RESOURCES TABLE

REAGENT or RESOURCE	SOURCE	IDENTIFIER
Antibodies		
ALKBH5	Sigma	Cat#HPA007196; RRID:AB_1850461
AXL	Cell Signaling Technology	Cat#8661; RRID:AB_11217435
Phospho-Src(Tyr416)	Cell Signaling Technology	Cat#6943; RRID:AB_10013641
Phospho-Erk1/2(Thr202/Tyr204)	Cell Signaling Technology	Cat#4370; RRID:AB_2315112
Phospho-Akt (Ser473)	Cell Signaling Technology	Cat#4060; RRID:AB_2315049
Phospho-Stat3(Tyr705)	Cell Signaling Technology	Cat#9145; RRID:AB_2491009
Phospho-PLCγ(Tyr783)	Cell Signaling Technology	Cat#14008; RRID:AB_2728690
ACTIN	Cell Signaling Technology	Cat#4967; RRID:AB_330288
GAPDH	Proteintech	Cat#60004-1-Ig; RRID:AB_2107436
KDM4C	Thermo Fisher	Cat#PA5-23065; RRID:AB_11152049
Pol II-CTD	Abcam	Cat#ab5095; RRID:AB_304749
H3K9me3	Abcam	Cat#ab8898; RRID:AB_306848
H3K4me3	Abcam	Cat#ab8580; RRID:AB_306649
H3	Abcam	Cat#ab1791; RRID:AB_302613
m^6A	Abcam	Cat#ab151230; RRID:AB_2753144
IgG	Proteintech	Cat#B900610; RRID:N/A
anti-human PE-CD11b	Biolegend	Cat#101208; RRID:AB_312791
anti-human FITC-CD34	Biolegend	Cat#343504; RRID:AB_1731852
anti-human APC-CD38	Biolegend	Cat#303510; RRID:AB_314362
anti-human APC-CD45	Biolegend	Cat#368512; RRID:AB_2566372
Anti-mouse CD4-APC	Biolegend	Cat#100412; RRID:AB_312697
Anti-mouse CD8a-FITC	Biolegend	Cat#100706; RRID:AB_312745
Anti-mouse CD11b-PE	Biolegend	Cat#101208; RRID:AB_312791
Anti-mouse CD3e-BV605	Biolegend	Cat#100351; RRID:AB_2565842
anti-Streptavidin APC-eFluor® 780	eBioscience	Cat#47-4317-82; RRID:AB_10366688
Anti-mouse CD3e-FITC	Biolegend	Cat#100204; RRID:AB_312661
Anti-mouse CD45.1-BV785	Biolegend	Cat#110743; RRID:AB_2563379
Anti-mouse CD127-BV650	Biolegend	Cat#135043; RRID:AB_2629681
Anti-mouse CD4-Biotin	Biolegend	Cat#100404; RRID:AB_312689
Anti-mouse Sca-1-Biotin	Biolegend	Cat#108103; RRID:AB_313340
Anti-mouse CD3e-Biotin	Biolegend	Cat#100304; RRID:AB_312669
Anti-mouse CD8a-Biotin	Biolegend	Cat#100704; RRID:AB_31274
Anti-mouse B220-Biotin	Biolegend	Cat#103204; RRID:AB_312989
Anti-mouse Gr-1-Biotin	Biolegend	Cat#108404; RRID:AB_313369
Anti-mouse CD127-Biotin	Biolegend	Cat#135005; RRID:AB_1953262
Anti-mouse Gr-1-APC-Cy7	BD	Cat#557661; RRID:AB_396775
Anti-mouse B220-PE-Cy5	BD	Cat#563103; RRID:AB_2738007
Anti-mouse CD16/32-BV605	BD	Cat#563006; RRID:AB_2737947
Anti-mouse CD48-BV510	BD	Cat#563536; RRID:AB_2738266
Anti-mouse CD45.2-PE-efluo610	eBioscience	Cat#61-0454-82; RRID:AB_2574562
Anti-mouse CD127-FITC	eBioscience	Cat#53-1271-82; RRID:AB_469909
Anti-mouse CD34-eFlour450	eBioscience	Cat#48-0341-82; RRID:AB_2043837
Anti-mouse Sca-1-APC	eBioscience	Cat#17-5981-83; RRID:AB_469488
Anti-mouse c-Kit-PE	eBioscience	Cat#12-1172-83; RRID:AB_465817

(*Continued on next page*)

Continued

REAGENT or RESOURCE	SOURCE	IDENTIFIER
Anti-mouse CD150-FITC	eBioscience	Cat#11-1501-82; RRID:AB_465209
Anti-mouse CD135-PE-Cy5	eBioscience	Cat#15-1351-82; RRID:AB_494219
Chemicals and Recombinant cytokines		
Recombinant Human IL-3	PeproTech	Cat#200-03
Recombinant Human SCF	PeproTech	Cat#300-07
Recombinant Human TPO	PeproTech	Cat#AF-300-18-10
Recombinant Human Flt3-Ligand	PeproTech	Cat#300-19
Recombinant Mouse SCF	PeproTech	Cat# 250-03
Recombinant Mouse IL-3	PeproTech	Cat# 213-13
Recombinant Mouse IL-6	PeproTech	Cat# 216-16
Puromycin	Merck	Cat#540411
Polybrene	Sigma-Aldrich	Cat#H9268
Actinomycin D	Sigma-Aldrich	Cat#A9415
StemSpan SFEM	STEMCELL Technologies	Cat#09655
Biological Samples		
Human AML Patient Samples	Tongji Medical College	N/A
Normal Human Bone Marrow Samples	Tongji Medical College	N/A
Cord blood	Tongji Medical College	N/A
Critical Commercial Assays		
MethoCult^{TM} GF H4434	STEMCELL Technologies	Cat#04434
MethoCult^{TM} GF M3434	STEMCELL Technologies	Cat#03434
Dual-Luciferase Reporter Assay System	Promega	Cat#1980
CD34 MicroBead Kit	Miltenyi Biotec	Cat#130-046-702
FITC Annexin V Apoptosis Detection Kit	BD Biosciences	Cat#556547
Human hematopoietic progenitor cell enrichment kit	STEMCELL Technologies	Cat#14056
Mouse Hematopoietic Progenitor Cell Isolation Kit	EasySep	Cat #19856c
Hoechst 33342	Thermo Fisher	Cat#H3570
NEBNext Poly (A) mRNA Magnetic Isolation Module	NEB	Cat#e7490
NEBNext Ultra Directional RNA Library Prep Kit	NEB	Cat#e7760
VAHTS^{TM} Small RNA Library Prep Kit for Illumina®	Vazyme	Cat#NR801
Library Preparation VATHS mRNA Capture Beads	Vazyme	Cat#N401-01
RNA Clean and Concentrator	Zymo research	Cat#R1013
protein-A beads	Thermo Fisher	Cat#10002D
TruSeq Stranded mRNA Library Prep Kit	Illumine	Cat#RS-122-2101
ReverTra Ace qPCR RT Kit	TOYOBO	Cat#FSQ-101
Deposited Data		
RNA-seq	This study	GEO: GSE128575
m^{6}A-seq	This study	GEO: GSE128575
SLAM-seq	This study	GEO: GSE128575
Ribo-seq	This study	GEO: GSE128575
Experimental Models: Cell Lines		
HEK293T	ATCC	CRL-3216; RRID:CVCL_0063
MOLM-13	DSMZ	ACC-554; RRID:CVCL_2119
THP1	ATCC	TIB-202; RRID:CVCL_0006
MV4:11	DSMZ	ACC-102; RRID:CVCL_0064
Experimental Models: Organisms/Strains		
NOD.Cg-*Prkdc*^{scid}*IL2rg*^{null} (B-NSG)	Biocytogen	N/A
Mouse: C57BL/6J	Jackson Laboratory	Cat#000664; RRID:IMSR_JAX:000664

(*Continued on next page*)

Continued

REAGENT or RESOURCE	SOURCE	IDENTIFIER
Mouse: *Mx1*-Cre	Jackson Laboratory	Cat#003556; RRID:IMSR_JAX:003556
Mouse: *Alkbh5*$^{fl/fl}$	Biocytogen	N/A
Mouse: B6.SJL	Jackson Laboratory	Cat#002014; RRID:IMSR_JAX:002014
Recombinant DNA		
pLKO.1	(Stewart et al., 2003)	Addgene Cat#8453
pLKO.1-SFFV-GFP	This study	N/A
LentiCRISPRv2	(Sanjana et al., 2014)	Addgene Cat#52961
pMIR-REPORT	ThermoFisher	Cat#AM5795
pMIR-REPORT-AXL	This study	N/A
LentiCRISPRv2-U6-shALKBH5#3′ -EF1a-ALKBH5-WT	This study	N/A
LentiCRISPRv2-U6-shALKBH5#3′ -EF1a-ALKBH5-H204A	This study	N/A
MSCV-MLL-AF9-YFP	(Zhang et al., 2018)	N/A
pCDH-CMV-Puro	SBI	Cat# CD513B
pCDH-AXL	This study	N/A
pCDH-ALKBH5	This study	N/A
Software and Algorithms		
GraphPad Prism 7	GraphPad Software	https://www.graphpad.com/
FlowJo software (version 8.5.2)	FlowJo	https://www.flowjo.com/
exomePeak (v2.16.0)	Bioconductor	http://bioconductor.org/packages/release/bioc/html/exomePeak.html
javaGSEA(v2.2.4)	Broad Institute	http://software.broadinstitute.org/gsea/index.jsp

RESOURCE AVAILABILITY

Lead Contact

Further information and requests for reagents may be directed to and will be fulfilled by the Lead Contact, Haojian Zhang (haojian_zhang@whu.edu.cn).

Materials Availability

Cell lines, plasmids and recombinant DNA used in this study are detailed in the Key Resources Table and available upon reasonable request. *Alkbh5*$^{fl/fl}$ mice will be provided upon reasonable request. All requests need to execute a suitable Materials Transfer Agreement.

Data and Code Availability

The accession numbers for the RNA-Seq, m^{6}A-Seq, SLAM-seq and Ribo-seq data reported in this paper were deposited in GEO under the accession number GEO: GSE128575.

EXPERIMENTAL MODEL AND SUBJECT DETAILS

Mice

C57BL/6J (CD45.2) background *Alkbh5*$^{fl/fl}$ and *Mx1*-cre mice were obtained from Biocytogen and the Jackson Laboratory, respectively. B6.SJL (CD45.1) and NOD.Cg-*Prkdc*^{scid}*IL2rg*^{null} (B-NSG) mice were purchased from the Jackson Laboratory and Biocytogen, respectively. All transgenic and knockout mice were CD45.2$^+$. Both male and female mice at 8-10 weeks old were used for experiments, with age- and gender-matched littermates as control. Congenic recipient mice (CD45.2) at 8-10 weeks old were used for AML transplantation, and CD45.1 recipients at 8-10 weeks old were used for normal hematopoietic transplantation assays. All mice were bred and maintained in Animal Center of Medical Research Institute at Wuhan University. All animal experiments were performed according to protocols approved by the Animal Care and Use Committee of Medical Research Institute, Wuhan University.

Primary AML patient and cord blood samples

All AML patient samples were collected from bone marrow aspirations at the time of diagnosis or relapse and with informed consent. In-house cohort included 88 AML patients (47 males and 41 females) representative of different subtypes by cytogenetics

classification, including patients with normal karyotype (n = 43), inv(16) (n = 11), *MLL*-rearranged t(11q23) (n = 12), and t(8,21) (n = 22). Samples were frozen in FBS with 10% DMSO and stored in liquid nitrogen. Normal cord blood units, designated for research use, were obtained from Tongji Medical College. Mononuclear cells (MNCs) were isolated by density gradient centrifugation with Ficoll (GE Healthcare Life Science). Human samples were randomly allocated to each experiment groups without predetermined sample size. All experiments involving human samples were conducted in compliance with all relevant ethical regulations and were approved by the Medical Ethics Committees of School of Medicine, Wuhan University.

Cell lines

The human acute leukemia cell lines (MOLM-13, THP1 and MV4:11) were maintained in Roswell Park Memorial Institute 1640 medium (RPMI-1640) with 10% FBS, 100 IU mL^{-1} penicillin and 100 μg mL^{-1} streptomycin. HEK293T were cultured in DMEM (Hyclone), supplemented with 10% FBS and 1% penicillin/streptomycin.

Primary cell culture

Primary AML patient-derived Lin^-CD34^+ cells were cultured in StemSpan SFEM (StemCell Technologies) supplemented with rhIL3 (20ng/mL), rhFLT3L (100ng/mL), rhTPO (50 ng/mL), rhSCF (100ng/mL), 1% penicillin–streptomycin (Sigma), and 2mM glutamine (Sigma). Cord blood-derived $CD34^+$ cells were cultured in StemSpan SFEM (StemCell Technologies) supplemented with rhSCF (100 ng/mL), rhFLT3L (100 ng/mL), rhTPO (50 ng/mL) and 1% penicillin–streptomycin (Sigma). All the cytokines were purchased from Peprotech.

METHOD DETAILS

Plasmids and lentivirus production

Lentivirus pLKO.1, pCDH-CMV-Puro, LentiCRISPRv2 vectors were used. All the target sequences for shRNA and sgRNA were listed in the Supplementary Information Table S1. The short hairpin RNA constructs against *ALKBH5, KDM4C, MYB* and *AXL* were designed and cloned in pLKO.1 according to instructions. The sgRNAs for ALKBH5 were cloned into pLentiCRISPRv2 according to instructions. For the ALKBH5 rescue experiment, human ALKBH5 cDNA was cloned into vector following shALKBH5#3′ which targets 3′UTR of ALKBH5. Enzymatic activity mutant ALKBH5 (H204A) was generated using Q5 Site-Directed Mutagenesis Kit (NEB E0554). AXL-3′UTR was cloned by PCR using primers CGACGCGTGACAACCCTCCACCTGGTACTC and CCCAAGCTT TCGTTGA TATACAAAGTTTTATG, and then inserted into pMIR-REPORT luciferase vector using restriction sites Mlu I and Hind III. For the overexpression of AXL and ALKBH5, pCDH-CMV-Puro was first modified to pCDH-CMV-Blast and then AXL and ALKBH5 cDNA was cloned by standard molecular cloning methods. Lentiviruses were produced in HEK293T cells transfected using calcium phosphate with viral packaging constructs pMD2.G and pSPAX2. Viral supernatants were harvested at 48 and 72 hours after transfection, and filtered through a 0.45 μm low protein binding membrane (Millipore).

Cell proliferation and *in vitro* colony-forming assay

For leukemia cell proliferation assays, AML patient-derived $CD34^+$ cells or human leukemia cells (THP1, MV4:11 and MOLM-13) were transduced with lentivirus and selected with 2 μg/ml puromycin for 2 days. After selection, cells were seeded into 24-well plates at the concentration of 20,000 cells per well in triplicates. Cell proliferation was assessed by counting cell numbers every 48 hours. For colony-forming assay, transduced AML patient-derived primary $CD34^+$ cells or cord blood-derived $CD34^+$ cells were plated in methylcellulose medium (MethoCult H4434; StemCell Technologies) according to the manufacturer's instructions, and mouse BM cells were cultured in MethoCultTM M3434 (STEMCELL Technologies) methylcellulose medium. For cell lines, transduced cells were plated in triplicate in 1.2% methylcellulose medium supplemented with 100 IU/mL penicillin and 100 μg/mL streptomycin, 10% FBS. Colonies were evaluated and scored after 7-12 days of incubation.

m^6A dot blot and quantification assay

For m^6A dot blot, total RNA was extracted from cell aliquots using TRIzol. RNA samples were quantified by nanodrop and UV cross-linked to the membrane, and membrane was blocked with 5% nonfat dry milk (in 1X TBS) for 1-2 hours and incubated with a specific anti-m^6A antibody (1:2000 dilution, Synaptic Systems, 202003) overnight at 4°C. HRP-conjugated secondary antibodies was added to the blots for 1 hour at room temperature and the membrane was developed with ECL Western Blotting Substrate (Bio-Rad) and exposure with X-Ray Super RX Films (Fujifilm). For m^6A quantification, m^6A level in mRNA was measured by EpiQuik m^6A RNA Methylation Quantification Kit (Colorimetric) (Epigentek) following the manufacturer's protocol.

Generation and analysis of murine MLL-AF9 leukemia model

Bone marrow cells were extracted from 8 to 10 weeks old *Alkbh5*$^{-/-}$ and WT mice, lineage negative cells (Lin^-) were enriched with hematopoietic stem/progenitor cell enrichment kit, and infected with MSCV-*MLL-AF9*-IRES-YFP retroviruses twice in the presence of 8 μg/mL Polybrene,10 ng/mL IL-3, 10 ng/mL IL-6, 20 ng/mL *SCF.* Infected cells (2×10^5-3×10^5) were transplanted into sub-lethally (7.5Gy) irradiated C57BL/6J mice by tail vein injection. Secondary transplantation was performed with 2,000 YFP^+ leukemia cells from bone marrow of leukemia mice. The YFP^+ leukemia cells in peripheral blood were analyzed every week. For the limiting dilution analysis, 5×10^5, 1×10^5, 2×10^3, 4×10^2 YFP^+ leukemia cells were transplanted to sub-lethally (7.5Gy)

irradiated C57BL/6J mice. The frequency of LSCs was analyzed by ELDA software (http://bioinf.wehi.edu.au/software/limdil). For AML maintenance assay, 8 to 12 weeks old *Alkbh5*$^{fl/fl}$ or *Alkbh5*$^{fl/fl}$;*Mx1*-Cre mice were sacrificed to generate leukemia cells. Bone marrow-derived leukemia cells were obtained from the primary recipients, and 2,000 YFP$^+$ leukemia cells were sorted and transplanted into the secondary recipients. Fourteen days after transplantation, recipients were intraperitoneally injected with 20-25 μg pIpC (InvivoGen) in PBS for 3 times to induce *Alkbh5* deletion.

In Vivo Xenograft Assay

AML patient-derived CD34$^+$ cells were cultured overnight as described above, and were transduced with lentivirus encoding shALKBH5 or shControl in the presence of 8 μg/mL polybrene. After 24h, percentages of GFP$^+$ cells were analyzed by flow cytometry, and equal number of GFP$^+$ cells (2x10^5) were transplanted into sub-lethally irradiated (2 Gy) NSG mice (8-10 weeks old). Twelve weeks after transplantation, human leukemia cells in peripheral blood (PB) and bone marrow were analyzed using APC-anti-human CD45 antibody by flow cytometry.

To determinate leukemia-initiating capacity of human leukemia cell lines THP1 and MOLM-13, cells were transduced with indicated lentiviruses, and selected using 2 μg/mL puromycin for 2 days. 5x10^5 selected cells were injected via tail vein into sub-lethally irradiated (2 Gy) NSG mice (8-10 weeks old). Recipient mice were monitored for survival.

Competitive repopulation assay

5 × 10^5 donor BM cells obtained from 8 to 10 weeks old donor Alkbh5$^{-/-}$ or WT mice were mixed with 5 × 10^5 competitor cells from CD45.1 mice, and transplanted into lethal irradiate (10Gy) CD45.1$^+$ recipients followed by analysis of repopulation and multiple lineage of donor cells 4,8,12, 16 weeks after transplantation. After 16 weeks, donor-derived BM cells were further analyzed with FACS, and LSK (Lin$^-$Sca-1$^+$cKit$^+$) cells were sorted to perform secondary transplantation (2,000 LSK per recipient).

Flow cytometry analysis and cell sorting

For isolating human leukemia stem/progenitor cells enriched CD34$^+$ cells using in lentivirus transduction experiments, freshly isolated or freshly thawed AML patient-derived and cord blood-derived mononuclear cells were used, and CD34$^+$ cells were enriched by positive selection using CD34 microbeads and a magnetic cell sorting system (Miltenyi). To sort leukemia stem cells (LSCs, Lin$^-$CD34$^+$CD38$^-$) and leukemia progenitor cells (LPCs, Lin$^-$CD34$^+$CD38$^+$), freshly isolated or freshly thawed AML patient-derived mononuclear cells were incubated with a lineage cocktail consisting of anti-human CD2, CD3, CD14, CD16, CD19, CD24, CD56, CD66b, glycophorin A, and Lin$^-$ immature cells were first enriched using human hematopoietic progenitor cell isolation kit (StemCell Technology, 14056). After washing, cells were stained with FITC-CD34 and APC-CD38 antibodies.

For mouse HSPC experiments, BM cells were lysed with RBC to remove red blood cells, the rest of cells were first stained with biotin-conjugated anti-CD4,anti-CD11b, anti-CD8a,anti-CD3e, anti-Gr-1, anti-B220,together with PE-anti-c-Kit, APC-anti-Sca-1, PE-Cy5-anti-CD135,BV605-anti-CD16/32, eFlour450-anti-CD34, BV650-anti-CD127, BV510-anti-CD48, FITC-anti-CD150. Biotin-conjugated antibodies were then stained with APC-eFlour780-anti-streptavidin. For analysis of mature cells, BM cells are stained with APC-anti-CD4,FITC-anti-CD8,PE-Cy5-anti-B220,PE-anti-CD11b, APC-Cy7-anti-Gr-1. To distinguish CD45.2$^+$ donor-derived cells in PB and BM, BV785-anti-CD45.1 and PE-efluo610-CD45.2 were added. To analyze LSCs in BM, red blood cells were removed by RBC lysis buffer, the rest of cells were first stained with biotin-conjugated anti-CD4, anti-CD8a,anti-CD3e, anti-Gr-1, anti-B220,anti-Sca-1, together with PE-anti-c-Kit, PE-Cy7-CD16/32, APC-anti-CD34, biotin-conjugated antibodies were then stained with APC-eFlour780-anti-streptavidin. Cell surface markers for different populations: LT-HSC (Lin$^-$Sca-1$^+$c-Kit$^+$CD135$^-$CD48$^-$CD150$^+$); ST-HSC (Lin$^-$Sca-1$^+$c-Kit$^+$CD135$^-$CD48$^-$CD150$^-$); MPP2 (Lin$^-$Sca-1$^+$c-Kit$^+$CD135$^-$CD48$^+$CD150$^+$); MPP3 (Lin$^-$Sca-1$^+$c-Kit$^+$CD135$^-$CD48$^+$CD150$^-$); MPP4 (Lin$^-$Sca-1$^+$c-Kit$^+$CD135$^+$CD48$^+$CD150$^+$); LMPP (Lin$^-$Sca-1$^+$c-Kit$^+$CD135$^+$CD127$^+$); GMP (Lin$^-$Sca-1$^-$c-Kit$^+$CD16/32^{hi}CD34$^+$); CMP (Lin$^-$Sca-1$^-$c-Kit$^+$CD16/32^{mid}CD34$^+$); MEP (Lin$^-$Sca-1$^-$c-Kit$^+$CD16/32^{low}CD34$^-$); CLP (Lin$^-$Sca$^-$1^{low}c-Kit^{low}CD135$^+$CD127$^+$); LSC (YFP$^+$Lin$^-$Sca-1$^-$c-Kit$^+$CD16/32^{hi}CD34$^+$).

Leukemia cells were stained with Hoechst 33342 to analyze cell cycle using flow cytometry. To analyze apoptosis, cells were stained with annexin V, and 7AAD was added before flow cytometic analysis. Differentiation assay was analyzed by staining cells with anti-human APC-CD11b. All flow cytometric analysis and cell sorting were performed on the BD Fortessa^{TM} X-20 or BD FACS Aria^{TM} III in the Core Facility of Medical Research Institute, Wuhan University, and data were analyzed with FlowJo software.

DNA pull-down assay

Two hundred million MOLM-13 cells were used. After washing once with cold PBS buffer containing inhibitors (PBSI, 0.5mM PMSF, 25mM β-glycerophosphate, 10mM NaF), cell pellets were lysed with 300μL of buffer A (10mM HEPES, pH7.9, 1.5mM MgCl2, 10mM KCl, 300mM sucrose, 0.5% NP-40). Following incubated on ice for 10 min, the lysates were centrifuged at 2,600 g for 30 s and sonicated with 150μL of buffer B (20mM HEPES, pH7.9, 1.5mM MgCl2, 420mM NaCl, 0.2mM EDTA, 2.5% glycerol). The samples were centrifuged at 10,400 g for 5 min, and the supernatants were incubated with 8μg of biotinylated DNA overnight at 4°C. Anti-biotin beads were used to incubate with samples for 2 to 4 h at 4°C. The pull-down proteins were eluted for mass spectrometry or western blotting.

Mass Spectrometry

Proteins in gels were reduced with 10mM DTT for 40 min at 56°C and subsequently alkylated with 50mM iodoacetamide for 30 min in the dark. Gel pieces were re-swollen on ice following dropwise addition of 10-20μL TEAB containing 10 ng/μL trypsin (Promega), and

the proteins were digested overnight at 37°C. Afterward, peptides were desalted with C18 cartridge and dried by vacuum centrifugation. Shotgun proteomics analyses were performed using an EASY-nLCTM 1200 UHPLC system (Thermo Fisher) coupled with an Orbitrap Q Exactive HF-X mass spectrometer (Thermo Fisher) operating in the data-dependent acquisition (DDA) mode. The detailed solvent gradient listed as follows: 5%–10% B, 2 min; 10%–30% B, 19 min; 30%–50% B, 2 min; 50%–90% B, 2 min; 90%–100% B, 5 min. Protein with at least 1 unique peptide was identified at FDR less than 1.0% on peptide and protein level, respectively. Proteins containing similar peptides and could not be distinguished based on MS/MS analysis were grouped separately as protein groups.

ATAC-sequencing

MOLM-13 cells (5×10^4) were pelleted by centrifugation at 500 g for 5 min at 4°C. All supernatants were removed carefully. Fifty microliters of transposase mixture (25μL of 2 × TD buffer, 1μL of Tn5, 0.5μL of 1% digitonin, and 23.5μL of nuclease-free water) were added to the cells, and the cell pellets were disrupted by pipetting. Transposition reactions were incubated at 37°C for 30 min with agitation at 300 rpm. Transposed DNA was purified using a QIAGEN MinElute Reaction Cleanup kit (28204), and purified DNA was eluted in 10 μL of elution buffer (10mM Tris-HCl, pH8). Transposed fragments were amplified and purified. Libraries were quantified using qPCR before sequencing. ATAC libraries were sequenced using 150bp paired-end read, dual-index sequencing on a Nova-Seq instrument.

RNA-seq and m^{6}A-seq and data analysis

For RNA-seq, total RNA was isolated using Trizol reagent (Thermo Fisher). Poly (A) mRNA was subsequently purified from 1 μg total RNA using NEBNext Poly (A) mRNA Magnetic Isolation Module. NEBNext Ultra Directional RNA Library Prep Kit (NEB, #E7760) was used for library preparation. RNA libraries were sequenced on an Illumina Hiseq X Ten platform with paired-end reads (150-bp read length). RNA-seq data were quantified with Kallisto (v0.43.1) and summarized to gene level by tximport (v1.10.1). EdgeR (v3.24.3) was employed for data normalization and differential expression analysis of RNA-seq counts.

For m^{6}A-seq, total RNA was extracted, and poly (A) mRNA was purified from 60 μg total RNA using the Library Preparation VATHS mRNA Capture Beads (Vazyme, N401-01). RNA samples were fragmented into ~100bp-long fragments by fragmentation buffer (10 mM ZnCl2, 10 mM Tris-HCl, pH 7.0). The fragmentation reaction was stopped with 0.05 M EDTA. Fragmented RNA was incubated for 2h at 4 °C with 1.5 μg of affinity purified anti-m^{6}A polyclonal antibody (Abcam, ab151230) in IP buffer (150 mM NaCl, 0.1% NP-40, 10mM Tris-HCl, pH 7.4). The mixture was then immunoprecipitated by incubation with protein-A beads (Thermo Fisher, 21348) at 4 °C for an additional 2 h. The beads were then separated and washed with 1x IP buffer three times before eluted with m^{6}A elution buffer for two times. The eluates were combined and purified with RNA Clean and Concentrator (Zymo, Orange, CA). The purified mRNA fragments were then used to construct libraries with TruSeq Stranded mRNA Library Prep Kit (Illumina, San Diego, CA). Sequencing was carried out on Illumina HiSeq X Ten. Reads from mRNA input and m^{6}A IP sequencing libraries were aligned to GRCh38 human reference genome with HISAT2 (v2.1.0). The m^{6}A peaks were called by exomePeak (v2.16.0). Differential RNA methylation analysis was performed according to a previous protocol (Meng et al., 2014). The distribution m^{6}A peaks over different regions on the transcript was depicted with annotations generated by PAVIS. RNA sequence motifs enriched in m^{6}A peaks were identified with DREME. The meta-profiles of m^{6}A sequencing data were generated with Deeptools (v2.0). Functional enrichment analysis were performed with DAVID tool (v6.8) and visualized by clusterProfiler (v3.10.1) (Huang et al., 2009; Yu et al., 2012). Gene Set Enrichment Analysis (GSEA) was performed with javaGSEA (v2.2.4) (Mootha et al., 2003; Subramanian et al., 2005). For visualizing m^{6}A peaks, .bigwig files were loaded in IGV (v2.4) and adjusted to the same scale.

SLAM-seq and data analysis

SLAM-seq libraries were prepared as previously described (Herzog et al., 2017). Cells were labeled with 100μM 4^{s}U (Sigma) for 1h and then washed twice with 1 × PBS and incubated with standard medium supplemented with 10mM uridine (Sigma). Cells collected at indicated time points were extracted using TRIzol. NEBNext Ultra Directional RNA Library Prep Kit (NEB, #E7760) was used for library preparation. RNA libraries were sequenced on an Illumina Hiseq X Ten platform with paired-end reads (150-bp read length). For Slam-seq analysis, cleaned sequencing data were submitted to SlamDunk (v0.2.4) with some little modifications. Briefly, reads were aligned to human genome GRCh38. T > C conversions were called and masked for SNPs. The base-quality cutoff is 28. And all reads were filtered for having $\geq$ 2 T > C conversions.

RIBO-seq and data analysis

RIBO-seq libraries were prepared as previously described (Reid et al., 2015). Briefly, three millions THP1 cells were lysed with 300μl lysis buffer (4mM $CaCl_2$, 10mM MgCl, 25 mM K-HEPES pH7.2, 200mM KOAc and 1% NP-40) for 5 min on ice and then centrifuged at 9,000 rpm for 5 min. Collected supernatant and 100μL of lysate were mixed with TRIzol and saved as input. KOAc concentration of the lysate was adjusted to 100mM by 1:1 dilution with water and then incubated with 10μg/mL micrococcal nuclease for 30 min at 37°C. RNA was extracted with TRIzol. Followed by PNK treatment, ribosome-protected fragments (RPFs), 25 to 40 nucleotides long, were purified with 15% TBE-Urea Gel. Libraries were then prepared using the VAHTS™ Small RNA Library Prep Kit for Illumina® following manufacturer's instructions. Libraries were sequenced with the Illumina HiSeq platform in a 50 bp single-end mode. For input samples, libraries were prepared as RNA-seq and sequenced on an Illumina Hiseq X-Ten platform with paired-end reads (150-bp read length). For ribo-seq analysis, cleaned sequencing data was counted at gene level by kallisto (v0.43.1). Gene counts data was then analyzed by R package Riborex to obtain differential translational efficiency.

Public database analysis

Briefly, the ATAC-seq count file were downloaded from NCBI Gene expression Ominibus (GEO) under the accession GSE74912, then subjected to unsupervised clustering analysis. Functional enrichment analysis was performed with clusterProfiler. The data accessible at GEO database accession GSE61022 and GSE60193 were processed and analyzed for different chromatin accessibility and histone modifications in whole genome, active genes, m^6A modifiers, and silent genes. Normalized ATAC-seq and ChIP-seq signals per gene were calculated with an *ad hoc* R script. Active genes were defined as top quartile expressed genes and silent genes were defined as bottom quartile expressed genes. The Cancer Genome Atlas (TCGA) AML datasets were used for survival and gene expression correlation analysis. RNA-seq datasets for a cohort with 436 AML cases (GSE16432) and a cohort with 134 AML cases (GSE83533) were used for survival analysis and correlation analysis between disease-free survival time and *ALKBH5* expression. GSE30285 and GSE34184 were used for estimate *ALKBH5* gene expression levels among multiple types of acute myeloid leukemia with healthy control. DHS-seq, Hi-C, CTCF ChIA-pet, Pol II ChIA-pet and multiple ChIP-seq data of the K562 cell from Encyclopedia of DNA Elements (ENCODE) (ENCODE Project Consortium, 2012) was downloaded and visualized in IGV (v2.4) and 3D Genome Browser (Wang et al., 2018).

Luciferase reporter assay

293T cells seeded in 24-well plates were transfected with the pMIR-REPORT luciferase vector fused with or without the *AXL*-3′UTR. Transfection efficiency was quantified by co-transfection with an actin promoter-driven Renilla luciferase reporter. The activities of firefly luciferase and Renilla luciferase in each well were calculated by a dual-luciferase reporter assay system (Promega). The ratios between the *AXL* 3′UTR reporter and Renilla control were determined 48hr after shRNA treatment. The relative luciferase activities were further normalized to that in cells transfected with the firefly luciferase vector control under the same treating conditions.

RNA decay assay

Cells were treated with actinomycin D at a final concentration of 5 μg/mL for indicated time and collected. Total RNA was extracted by TRIzol and analyzed by RT-PCR. GAPDH was used as endogenous control. The half-life of mRNA was estimated according to previously described (Chen et al., 2008). The rate of disappearance of mRNA concentration at a given time (dC/dt) is proportional to both the rate constant for decay (k_{decay}) and the cytoplasmic concentration of the mRNA (C). This relation is described by the following equation:

$$dC/dt = -k_{decay}C$$

The minus symbol indicates that the mRNA is being degraded. This relationship leads to the derivation of the equation: where C_0 is the concentration of the mRNA at time 0, before decay starts.

$$\ln/(C/C_0) = -k_{decay}t$$

To determine the half-life ($t_{1/2}$), this means $C/C_0 = 1/2$. Rearrangement of equation above leads to the following equation:

$$\ln(1/2) = -k_{decay}t_{1/2}$$

from where:

$$t_{1/2} = \ln 2/k_{decay}$$

Quantitative RT-PCR

Total RNA from leukemia cells was purified using TRIzol (Life Technologies) according to the manufacturer's instructions. One microgram of purified total RNA was retrotranscribed using the ReverTra Ace qPCR RT Kit (TOYOBO). The levels of specific RNAs were measured using Bio-Rad real-time PCR machine and Fast SybrGreen PCR mastermix according to the manufacturer's instructions. Primer sequences are listed in the Supplementary Information Table S1. The $2^{-\Delta\Delta Ct}$ method was used to normalize expression to GAPDH and ACTB for cell lines.

Chromatin immunoprecipitation (ChIP)-qPCR assays

AML patient-derived leukemia cells or human leukemia cell lines (MOLM-13, THP1) cells were cross-linked with 1% formaldehyde at room time for 10 min. The reactions were stopped using 0.125M glycine and incubated for 5 min at room temperature. After cell lysing, cross-linked chromatin was sheared using a sonicator. The 2 μg of anti-ALKBH5 (sigma), anti-KDM4C, anti-Pol II-CTD, and anti-H3K9me3, or control IgG antibodies were used for immunoprecipitation. After eluting DNA from the precipitated immune complex, DNA gel electrophoresis or quantitative real-time PCR (qPCR) analysis was performed. For the input control, 1% of the sonicated DNA was directly purified before immunoprecipitation and subjected to PCR with the same primers.

RIP-PCR

MOLM-13 cells were crosslinked by UV (stratalinker 1800 (254nm),400Mj/cm2). Nuclear extraction was isolated and sonicated. 2 μg of ALKBH5 antibody or a corresponding control rabbit IgG (AP132, Sigma) was conjugated to protein A/G magnetic beads

(Thermo Fisher Scientific) by incubated for 4h at 4 °C, and with pre-cleared nuclear extraction in RIP buffer (25mM Tris-HCl, 150mM KCL, 5mM EDTA, 0.5% NP40, 0.5mM DTT, 1 × protease inhibitor, 1 × RNase inhibitor) at 4 °C overnight. After washing with RIP buffer for five times, beads were resuspended in 80 μL PBS, followed by DNA digestion at 37 °C for 15 min and incubated with 2 μL (20 mg/mL) of proteinase K (Thermo Fisher) at 55 °C for 30min. Input and co-immunoprecipitated RNAs were recovered by TRIzol, extraction and analyzed by qPCR .

Western blot analysis

Cells were lysed in RIPA with protease inhibitor cocktail (Roche), and the total cell lysates were resolved with SDS-PAGE gels. Membranes were blocked for 30min at room temperature in TBS supplemented with 5% non-fat dried milk, and incubated overnight at 4°C with primary antibody diluted in the same blocking buffer. After three washes in TBST, membranes were incubated for 1h at room temperature with horseradish peroxidase (HRP)-conjugated secondary antibodies diluted in blocking buffer, then washed a further three times with TBST before incubation with ECL Western Blotting Substrate (Bio-Rad) and exposure with X-Ray Super RX Films (Fujifilm).

QUANTIFICATION AND STATISTICAL ANALYSIS

The Student's t test was used for significance testing. The log-rank test was used to compare survival curves. P values of less than 0.05 were considered statistically significant. Statistical analyses were performed using GraphPad Prism 7.0 or the R statistical environment. In the figures, asterisks indicate *$p < 0.05$, **$p < 0.01$, and ***$p < 0.001$.